

EFFECTS OF PRIOR HAMSTRING INJURY ON MORPHOLOGY, FUNCTION,
AND MECHANICS

by

Amy Silder

A dissertation submitted in partial fulfillment of
the requirements for the degree of

Doctor of Philosophy
(Biomedical Engineering)

at the

UNIVERSITY OF WISCONSIN-MADISON

2009

UMI Number: 3383953

Copyright 2009 by
Silder, Amy

All rights reserved

INFORMATION TO USERS

The quality of this reproduction is dependent upon the quality of the copy submitted. Broken or indistinct print, colored or poor quality illustrations and photographs, print bleed-through, substandard margins, and improper alignment can adversely affect reproduction.

In the unlikely event that the author did not send a complete manuscript and there are missing pages, these will be noted. Also, if unauthorized copyright material had to be removed, a note will indicate the deletion.

UMI[®]

UMI Microform 3383953
Copyright 2009 by ProQuest LLC
All rights reserved. This microform edition is protected against
unauthorized copying under Title 17, United States Code.

ProQuest LLC
789 East Eisenhower Parkway
P.O. Box 1346
Ann Arbor, MI 48106-1346

A dissertation entitled

**Effects of Prior Hamstring Injury
on Morphology, Function, and Mechanics**

submitted to the Graduate School of the
University of Wisconsin-Madison
in partial fulfillment of the requirements for the
degree of Doctor of Philosophy

by

Amy Silder

Date of Final Oral Examination: July 28th, 2009

Month & Year Degree to be awarded: **December** **May** **August** 2009

Approval Signatures of Dissertation Committee

Signature, Dean of Graduate School

Martin Cadwallader *AW*

Acknowledgements

Darryl Thelen, Bryan Heiderscheid, Manager Kelli Hellenbrand (and sometimes Sara),
Marc Sherry, Mike Tuite, Christopher Westphal, Master Ben Whittington, Scott Reeder,
and Silvia Blemker.

National Institutes of Health Grant Number AG 24276, National Institutes of Health
Grant Number R01 AR 56201, National Institutes of Health Grant Number
1KL2RR025012, National Football League Charities, National Science Foundation
Predoctoral fellowship (AS), Grant from the Tong Family Foundation, American Society
of Biomechanics Grant-In-Aid (AS),

EFFECTS OF A PRIOR HAMSTRING INJURY ON MORPHOLOGY, FUNCTION
AND MECHANICS

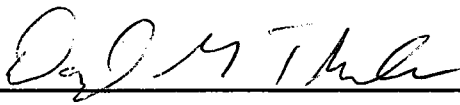
Amy Silder

Under the supervision of Associate Professor Darryl G. Thelen

at the University of Wisconsin-Madison

Hamstring strain injuries are common in sprinting related sports, and have a high re-injury rate. The majority these injuries occur along the proximal musculotendon junction (MTJ) of the biceps femoris long head (BFLH). The purpose of this dissertation was to investigate the long term effects of a prior hamstring strain injury on morphology and biomechanical function. Magnetic resonance (MR) imaging was used to quantify scar tissue and atrophy in the previously injured musculotendon many months following injury. To understand the influence of morphological changes on hamstring function, we tested the hypothesis that scar tissue would induce shifts in the active and passive force-length relationship, such that forces would be produced at effectively shorter lengths, when compared to the un-injured limb. A passive joint stiffness model was developed and used to measure bilateral differences in hamstring musculotendon stiffness in subjects with a prior injury. These same subjects participated in a sprinting assessment during which bilateral differences in muscle activities and musculotendon mechanics were measured. Finally, isokinetic knee flexion-extension strength was measured for each subject. Results revealed no significant differences in running kinematics or muscle activation patterns. A consistent shift in angle of peak torque during strength testing was

not revealed. However, the five subjects with the largest amount of scarring exhibited a 10° increase in the angle of peak torque compared to the un-injured limb, suggesting the degree of scarring may influence functional changes that take place. Thus, to understand the influence of prior injury on in-vivo hamstring muscle mechanics, a MR compatible device was designed and built to impose either elastic or inertial loads on the hamstrings, thereby enabling a comparison active-lengthening and relaxing-lengthening contractions. Cine phase contrast imaging was used to obtain hamstring muscle tissue velocities from eleven healthy and four subjects with prior hamstring injuries. Displacements and mechanical strains were estimated within a region that enclosed the BFLH. Peak first principal strains were greatest adjacent to the proximal MTJ and significantly greater in the previously injured subjects. We conclude that scar tissue may adversely affect local tissue mechanics in such a way that increases the risk for re-injury.



Darryl G. Thelen

Table of Contents

Acknowledgements	i
Abstract	ii
Table of Contents	iv
MR Observations of Long-Term Musculotendon Remodeling Following A Hamstring Strain Injury.....	1
Identification of Passive Elastic Joint Moment-Angle Relationships in the Lower Extremity	20
Influence of a Prior Hamstring Strain Injury on Strength, Flexibility, and Biomechanical Function	36
A MR-Compatible Loading Device for Dynamically Imaging Shortening and Lengthening Muscle Contraction Mechanics	54
The Influence of Prior Hamstring Injury on Lengthening Muscle Tissue Mechanics	71
Conclusions.....	90
References.....	94
Appendix A.....	100
Appendix B.....	103

Chapter 1

MR Observations of Long-Term Musculotendon Remodeling Following A Hamstring Strain Injury

Introduction

Muscle strain injuries may account for ~30% of sports medicine practice (Garrett, 1996), with hamstring injuries being particularly frequent among individuals participating in high speed running (Seward et al., 1993; Arnason, et al., 2004; Kujala et al., 1997; Orchard, 2001; Arnason et al., 2004). The treatment and rehabilitation of hamstring injuries remains challenging, as evidenced by approximately 30% of individuals experiencing a re-injury within the first year after initial injury (Orchard and Best, 2002; Orchard and Seward, 2002; Woods et al., 2004). Of particular clinical concern is the observation that subsequent injuries are often more severe and require more time away from sport than the initial injury (Brooks et al., 2006; Koulouris et al., 2007).

Magnetic resonance (MR) imaging provides an objective standard for confirming the presence of an acute muscle strain injury (Verrall et al., 2001; Koulouris and Connell, 2005). Recent studies have shown that the location and extent of abnormalities (e.g. edema and hemorrhage) on MR images not only confirm the presence and severity of initial muscle fiber damage, but can also provide a reasonable estimate of the rehabilitation period (Slavotinek et al., 2002; Connell et al., 2004; Gibbs et al., 2004). In addition, re-injury rates have been shown to be higher among individuals that sustain a

more severe original injury, as determined by the length of muscle damage present on MR images obtained at the time of injury (Verrall et al., 2006; Koulouris et al., 2007).

Various studies have investigated structural changes immediately following an acute hamstring strain injury (Garrett et al., 1989; Slavotinek et al., 2002; Connell et al., 2004; Koulouris et al., 2007). However, it is unclear how repair processes may alter musculotendon morphology in the months following return to sport. It has been hypothesized that scar tissue formation, along with weakness or atrophy of the previously injured muscle may be contributing factors to re-injury (Orchard and Best, 2002). Indeed, prior animal models of injury have shown that muscle tissue may not be able to fully regenerate to pre-injury state, with connective scar tissue persisting at the site of injury indefinitely (Kaariainen et al., 2000; Best et al., 2001). Given that most hamstring strain injuries occur along the proximal musculotendon junction (De Smet and Best, 2000), where the muscle fibrils intersect with the tendon (Garrett et al., 1989) (Fig. 1), it is likely that remodeling takes place near this region. In addition, atrophy and fatty replacement within the previously injured or surrounding muscles may also occur as part of the remodeling process (Tuite and DeSmet, 1994; Bordalo-Rodrigues and Rosenberg, 2005; Koulouris and Connell, 2005).

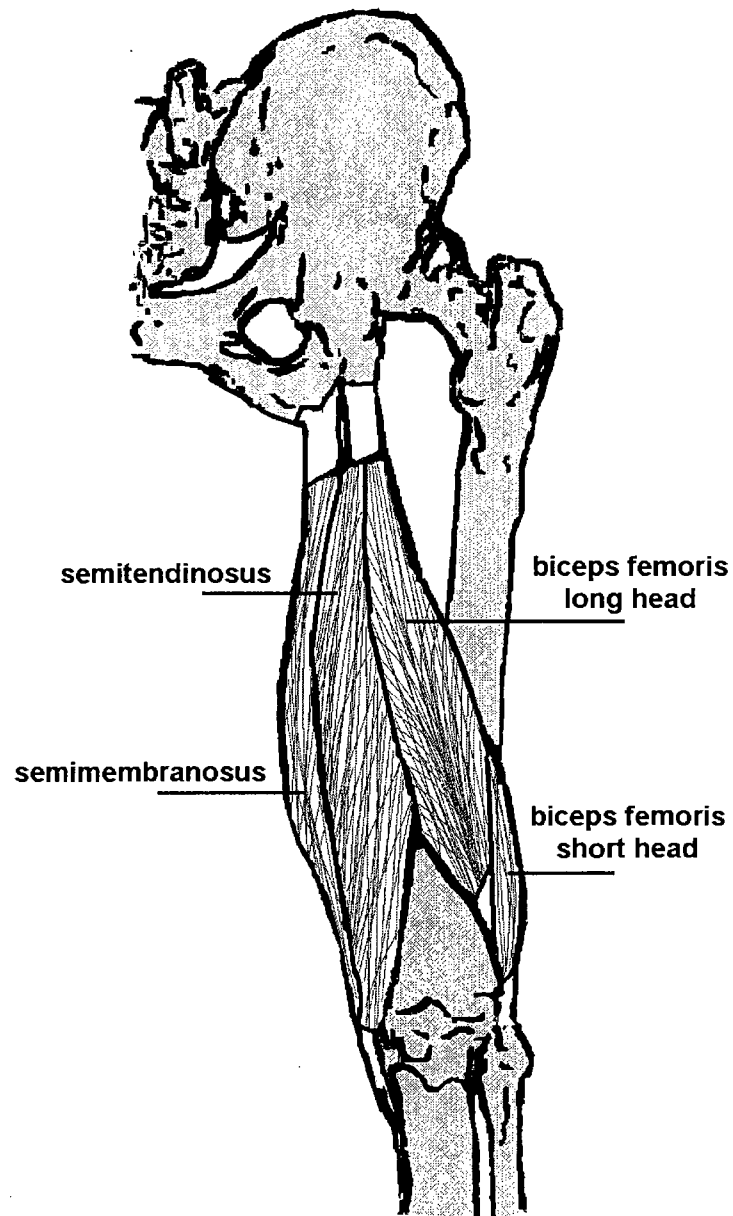


Figure 1: The hamstring muscles consist of the semimembranosus, semitendinosus, and biceps femoris muscles. They originate from an incompletely separated tendon on the lateral and proximal aspect of the ischial tuberosity. Of the three hamstring muscles, the long head of the biceps femoris is the most commonly injured (Garrett et al., 1989; Speer et al., 1993; Garrett, 1996; De Smet and Best, 2000).

The purpose of this study was to use MR imaging to qualitatively and quantitatively investigate evidence of long-term changes in muscle and tendon morphology after a hamstring strain injury. We hypothesized that scar tissue would be present near the site of prior injury, with accompanying atrophy of the previously injured muscle. MR images from healthy control subjects were also obtained in order to provide insights into normal variations in muscle and tendon morphology between limbs.

Materials and Methods

Fourteen previously injured athletes were recruited (Table 1). All had experienced a clinically diagnosed prior hamstring strain injury (grade I or II) that required a minimum of two weeks away from sport, and were free of other current or history of musculoskeletal impairments. Each subject participated in a supervised rehabilitation program, and since returned to sport for at least one month prior to this study. An additional five healthy athletes were recruited with no current or history of musculoskeletal impairments. In accordance with the UW Health Sciences Human Subjects' Committee, each subject or parent provided written informed consent prior to participation in the investigation.

Table 1. Demographics and information regarding the prior injury/injuries of the subjects participating in this study. Abbreviations: SM = semimembranosus; BF = biceps femoris, ST = semitendinosus.

Subject	Gender	Age	Months from Injury	Side of Injury	Location of Injury	Number of Injuries	Activity at Time of Injury
1	Male	44	23	Right	Proximal SM	1	Soccer
2	Male	18	5	Right	Proximal BF	1	Soccer
3	Female	43	9	Right	Proximal BF	2	Softball
4	Male	31	5	Left	Proximal BF	2	Football (sprinting)
5	Male	19	13	Left (both)	Proximal BF (both)	2	Track (sprinting)
6	Female	19	7	Left (both)	Proximal BF (both)	2	Track (hurdling)
7	Male	18	8	Right (all)	Proximal BF (all)	3	Track (sprinting)
8	Female	45	6	Right	Distal BF	1	10k race
9	Male	47	19	Left	Distal BF	1	Track (sprinting)
10	Male	56	18	Right	Distal BF	1	Sprinting
11	Male	20	7	Right	Distal BF	1	Track (sprinting)
12	Female	17	5	Right (both)	Distal BF (both)	2	Track (sprinting)
13	Male	38	5	Left (recent) Right (prior)	Distal ST (recent) Proximal BF (prior)	2	Soccer
14	Male	23	5	Right (recent) Right (prior)	Distal BF (recent) Proximal BF (prior)	2	Track (sprinting)

MR images were obtained of both limbs on a 1.5 Tesla MR scanner (General Electric Healthcare, Milwaukee, Wisconsin) using a phased-array torso coil. T2-weighted fast spin-echo coronal images were obtained for each subject (TR/TE_{eff}, 2200/70; matrix, 512x512; 2 NEX; 44cm FOV; 4/0.4mm thickness). T1-weighted fast-spin echo axial and coronal images were acquired for the first five previously injured subjects (TR/TE_{eff}, 550/17; matrix, 512x512; 1 NEX; 5mm axial with no gap, and 4.0/0.4mm coronal slice thickness). Thereafter, an iterative decomposition algorithm of water and fat with echo asymmetric and least-squares estimation (IDEAL) spoiled gradient echo sequence (Reeder et al., 2005) was used for the subsequent nine previously injured and five healthy subjects (TR/TE_{eff}, 12.7/4.4; 15° flip angle; matrix, 512x512; 1.5 NEX; 1.4mm coronal slice thickness, no gap). The change from a T1-weighted to IDEAL sequence was made because IDEAL uses a water-fat separation algorithm, such that reconstructed images do not suffer from water-fat chemical shift artifacts, thereby eliminating the need to manually account for this artifact, as was done for the T1-weighted images. Bilateral images were acquired from the ischial tuberosity to just below the knee, which encompassed the entire length of the biarticular hamstrings.

Qualitative bilateral comparisons were used to assess the presence of any fatty infiltration and differences in structure that may have arisen as a result of the previous injury. These qualitative comparisons were conducted by the same experienced musculoskeletal radiologist (M.J.T) for all subjects, who was blinded of the injury location during all assessments. An increased amount of high-intensity signal within muscle on T1-weighted sequences, compared to the contralateral limb, was indicative of

fatty replacement (Tuite and DeSmet, 1994). Scar tissue is represented as low-intensity signal on both T1- and T2-weighted MR images (Tuite and DeSmet, 1994; Drape et al., 1996; May et al., 2000; Best et al., 2001). We considered increased low-intensity signal adjacent to tendon on the previously injured limb to be potential evidence of scarring (Bordalo-Rodrigues and Rosenberg, 2005) as a result of the prior injury.

Hamstring muscle and tendon/scar volumes were determined for both limbs using manual segmentation. We quantified volumes of the biceps femoris long head (BFLH), biceps femoris short head (BFSH), proximal conjoint biceps femoris and semitendinosus tendon (PBFT) and proximal semimembranosus tendon (PSMT) (Mimics Software; Materialize Corp.; Ann Arbor, MI) (Fig. 2). For individuals with distinguishable proximal biceps femoris and semitendinosus tendons, only the biceps femoris tendon volume was quantified. Muscle or tendon boundaries were identified and manually outlined on each image in which the desired structure was present. Volumes were calculated as the product of the inter-slice distance and the summed cross-sectional areas from all slices containing the muscle or tendon of interest. All measurements were conducted for both the previously injured subjects and the healthy controls by the same investigator (A.S.), blinded to the site of injury. In addition, we conducted an inter-observer reliability test during which one of the investigators (D.G.T) manually segmented the muscles and tendons of the fourth control subject but was blinded to the subject being investigated during the segmentation process. Percent difference in muscle and tendon volumes between limbs were then calculated all subjects. Differences are reported relative to the un-injured limb for the previously injured subjects and relative to

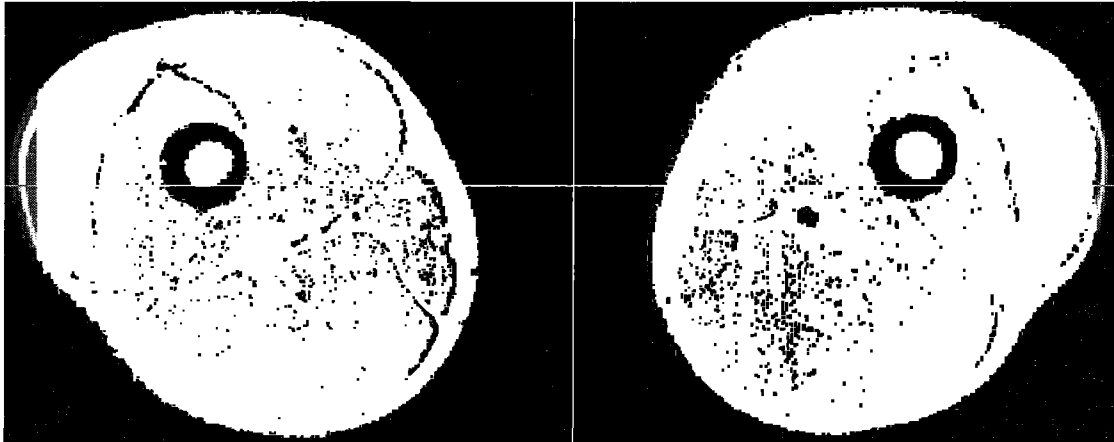


Figure 2: Hamstring muscles and tendons were manually outlined on each slice and used to estimate the muscle and tendon volumes of each limb. The right (left image) biceps femoris short head (purple), biceps femoris long head (blue), semimembranosus (orange), and semitendinosus (red) were outlined on this image, obtained from a previously injured subject.

the right limb for the control subjects. Volume difference measures were statistically evaluated between the previously injured and control subjects using t-tests ($\alpha=0.05$).

Results

Clinical notes indicated that seven subjects (1-7) sustained only proximal injuries, five subjects (8-12) sustained only distal injuries, and two subjects sustained both a proximal and distal injury (13,14) (Table 1). Twelve subjects injured only the biceps femoris, one subject injured the semimembranosus, and the remaining subject injured both the biceps femoris and semitendinosus (separate limbs on different occasions). Six of the subjects sustained a single injury, seven subjects sustained two injuries, and one subject experienced three injuries.

Differences in muscle and tendon volumes computed by the two investigators during the inter-observer reliability test revealed good agreement. BFLH and BFSH volume differences between limbs were identical for both investigators. Some

disagreement in tendon volume differences was present, with a 3% and 10% discrepancy between investigators for the PBFT and PSMT, respectively.

Biceps Femoris Injuries: Significant differences were observed between limbs for the BFLH volume of the 13 subjects with biceps femoris injuries, compared to the healthy controls ($p < 0.01$) (Table 2). These differences were represented by atrophy of the BFLH, often accompanied by hypertrophy of the BFSH (Fig. 3). Qualitative assessment identified that 10 of the 13 subjects presented with visual evidence of muscle volume differences. Additionally, the differences in PBFT volumes between limbs was larger for the previously injured subjects, compared to the controls, although not significant ($p = 0.07$). The measured differences for the previously injured subjects were detected by qualitative assessment in 11 of the subjects (Fig. 4). The mean percent difference between limbs in the BFLH, BFSH, and PBFT volumes for the 13 previously injured subjects was -10%, +13% and, +85%, respectively.



Figure 3: Moderate to substantial atrophy of the previously injured biceps femoris long head (BFLH) was present with corresponding hypertrophy of the biceps femoris short head (BFSH) in seven of the 13 subjects with biceps femoris injuries. Four of the remaining six subjects presented with either BFLH hypertrophy (2 subjects) or BFSH atrophy (2 subjects). Shown here, atrophy of the right BFLH along with hypertrophy of the right BFSH.

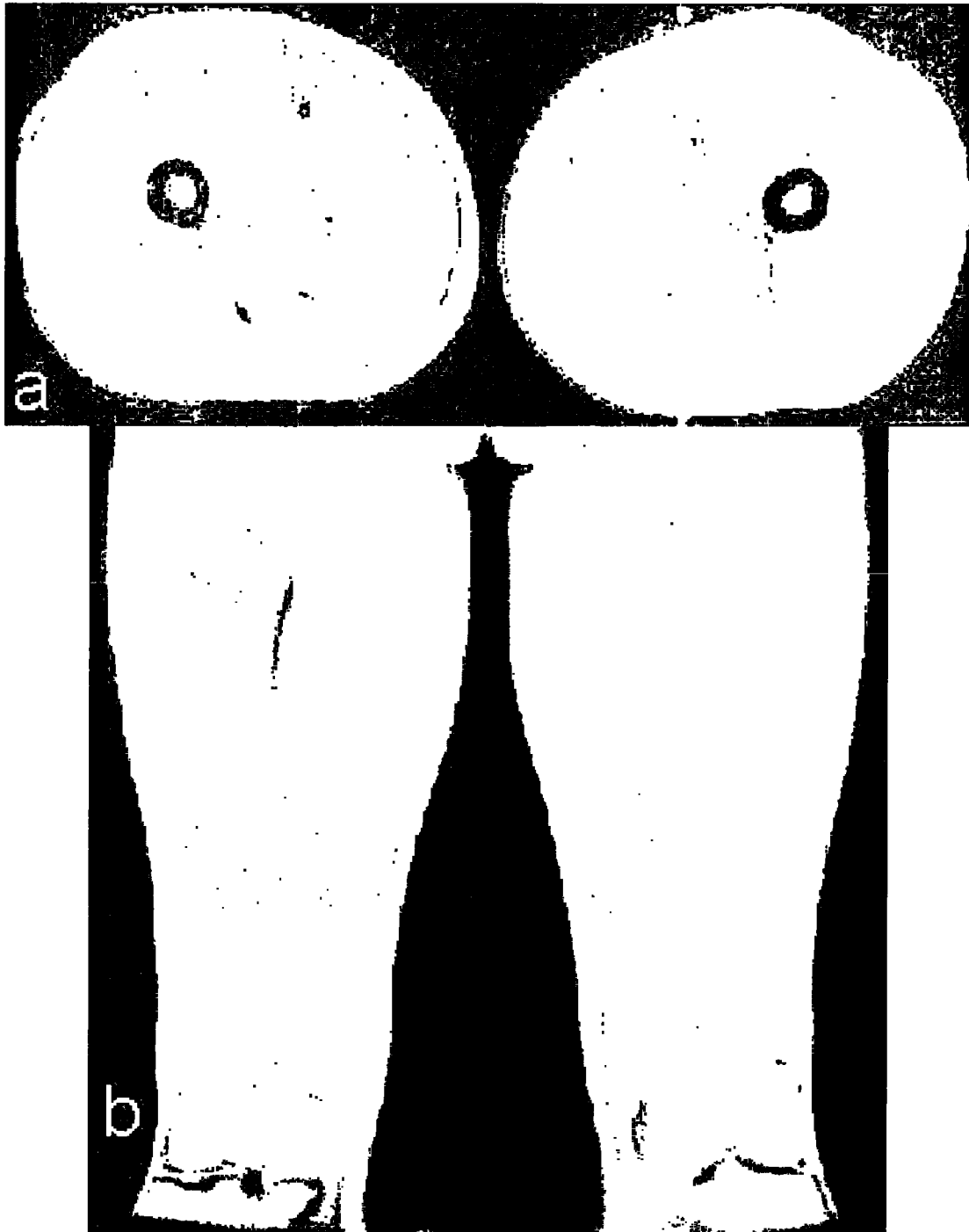


Figure 4: Scarring was present along the proximal musculotendon junction in four of the six subjects with proximal biceps femoris injuries. The arrow denotes an increased region of low-intensity signal along the proximal musculotendon junction of the biceps femoris in the axial (a) and coronal (b) planes.

Proximal Injuries: Seven subjects (1-7) sustained only proximal injuries. Four of these subjects experienced two injuries, two sustained one injury, and one subject had three injuries. Six of the seven subjects injured the proximal biceps femoris, while one injured the semimembranosus.

An increase in PBFT volume ($p=0.06$), atrophy of the BFLH ($p<0.01$), and hypertrophy of the BFSH ($p=0.06$) were present for the six subjects with proximal biceps femoris injuries, compared to the healthy controls (Table 2). Increased low-intensity signal was qualitatively observed along the musculotendon junction of the PBFT in four of these six subjects (Fig. 4). The PBFT volumes for these four subjects were, on average, 140% (range 105-218%) larger than the un-injured limb. Atrophy of the BFLH was qualitatively characterized on the axial images as decreased cross-sectional area of the proximal BFLH relative to the contralateral muscle (within 14-16 mm of the ischial tuberosity). Hypertrophy of the BFSH generally occurred near its origin, with the largest measured and observed differences occurring along the proximal lateral supracondylar line. Finally, subject 3 presented with substantial fatty infiltration within both the long and short heads of the biceps femoris on the previously injured limb (Fig. 5), with no visible or measurable scarring present.



Figure 5: Fatty infiltration was observed within the long and short heads of the biceps femoris. The white arrow denotes the previously injured BFLH, while the black arrow designates the BFLH on the un-injured limb.

The single subject with a semimembranosus injury exhibited a 52% increase in PSMT volume compared to the contralateral limb. A moderate increase in semimembranosus muscle volume (+10%) was found with no measurable or observable difference in biceps femoris muscle size.

Distal Injuries: Five subjects sustained only distal injuries, all to the biceps femoris. Four of these subjects (8-11) experienced single injuries, while one subject incurred two injuries. Atrophy of the BFLH ($p=0.01$) was present, compared to the healthy controls, with three of the subjects demonstrating moderate to substantial atrophy of the BFLH and/or hypertrophy of the BFSH (Fig. 3, Table 2). PBFT volume was similar ($p=0.38$) between subjects with and without prior injury. However, increased low-intensity signal was qualitatively observed along the distal musculotendon junction of the biceps femoris for all of these subjects. One of the subjects with a distal injury also presented with considerable fatty infiltration within both the long and short femoris on the previously injured limb (Fig. 5).

Table 2: Percent change in muscle and tendon volumes between the injured and non-injured limbs for the previously injured subjects and between the right and left limbs for the healthy controls. Negative values indicate the injured limb to be smaller than the non-injured limb, or that the right limb is smaller than the left limb. Abbreviations: BFLH = biceps femoris long head muscle; BFSH = biceps femoris short head muscle; PBFT = combined proximal biceps femoris and semitendinosus tendon; PSMT = proximal semimembranosus tendon; SM = semimembranosus muscle.

Case	Muscle volume			Tendon volume	
	BFLH	BFSH	SM	PBFT	PSMT
<i>Proximal SM injury</i>					
1	-2	+4	+10	-32	+52
<i>Proximal BF injury</i>					
2	-4	+23	---	+218	+8
3	-20	+30	---	0	-4
4	-23	+1	---	+114	-5
5	-12	+17	---	+124	+12
6	-16	+46	---	+105	+27
7	+5	+16	---	-7	-1
mean (SD)	-12 (11)	+22 (15)	---	+92 (85)	+6 (12)
p-value*	<0.01	0.06	---	0.06	0.66
<i>Distal BF injury</i>					
8	-26	+25	---	---	---
9	-29	+19	---	---	---
10	+1	+9	---	---	---
11	-4	-3	---	---	---
12	-6	+9	---	---	---
mean (SD)	-13 (14)	+12 (11)	---	---	---
p-value*	0.01	0.38	---	---	---
<i>Proximal & distal injury</i>					
13	+3	-21	---	-4	-46
14	-1	-1	---	+132	+7
<i>Healthy Controls</i>					
1	-13	-6	---	+9	+10
2	+2	+7	---	+12	+1
3	+2	+4	---	+7	+6
4	+14	+12	---	+18	+20
5	+18	+7	---	-4	+8
absolute mean (SD)	10 (7)	2 (3)	---	8 (8)	9 (7)

* compared to healthy controls

Proximal and Distal Injuries: Two subjects experienced both a proximal and distal injury (Table 1). Subject 13 injured his right proximal biceps femoris and left distal semitendinosus. Subject 14 injured both his right proximal and distal biceps femoris, but exhibited a much more substantial increase in tendon volume proximally, than distally (Table 2).

Healthy Controls: Three males and two females were recruited. The mean (SD) age, height, and weight of these subjects was 28 (5) years, 1.73 (0.06) m, 68 (4) kg, respectively. Some degree of asymmetry between the right and left limbs was observed for each subject (Table 2). Four of the five subjects exhibited larger BFLH and BFSH muscles in the right limb, while one subject had a larger left BFLH and BFSH. Four of the five subjects also had larger PBFT and PSMT tendons on the right limb, while one subject had a larger right PSMT and larger left PBFT.

Discussion

We qualitatively and quantitatively investigated long-term changes (5-23 months) in muscle and tendon morphology following a hamstring strain injury. Despite the diversity within our subject population (Table 1), we observed some consistency in the injuries sustained and the morphological changes that ensued. The BFLH was the most commonly injured muscle, consistent with the observations of prior studies (Garrett et al., 1989; Speer et al., 1993; Garrett, 1996; De Smet and Best, 2000). Evidence of scar tissue was often observed along the musculotendon junction adjacent to the site of prior injury. For those subjects with biceps femoris injuries, we also observed atrophy of the BFLH on the side of injury, often accompanied by hypertrophy of the BFSH.

In order to gain further insights into the natural variations that exist in muscle and tendon morphology in healthy individuals, we obtained images of five healthy control subjects. These subjects also showed some variability in muscle and tendon volumes between limbs. It is interesting to note that the previously injured subjects exhibited a significantly smaller BFLH and larger BFSH on the previously injured limb. In contrast, both the BFLH and BFSH were either smaller or larger than the contralateral limb for all five healthy subjects. We also observed substantial variations in tendon sizes between the limbs of healthy subjects, although to a much lesser degree than the previously injured subjects, particularly in the PBFT (PBFT: healthy, 14%; previously injured, 92%).

Scar tissue has been observed as early as six weeks after an initial injury (Connell et al., 2004), and the degree of PBFT asymmetry present in the previously injured subjects in this study demonstrate that scarring likely persists on a more long-term basis (5-23 months post injury). Unfortunately, we cannot definitively conclude if this persists indefinitely, as shown in animal models (Kaariainen et al., 2000; Best et al., 2001). It is important to recognize that, while asymmetries exist in healthy individuals, apparent thickening of a tendon, compared to the contralateral limb, on MR images may be indicative of a prior musculotendon injury. Scar tissue adjacent to the site of prior injury may alter in-vivo muscle contraction mechanics. In particular, the collagen fibers comprising remodeled tendon tend to be less well organized, with different stiffness properties than normal tendon (Butler et al., 2004). Specifically, scar tissue may increase the overall mechanical stiffness of the myofibrous tissue it replaces, which may require the muscle fibers to lengthen a greater amount to achieve the same overall

musculotendon length relative to a pre-injury state. Finally, six of the eight subjects in this study that sustained multiple injuries and incurred those injuries in the same leg and location (i.e. proximal or distal) as the previous injury, as noted on clinical exam. This supports previous hypotheses (Nikolaou et al., 1987; Koulouris and Connell, 2005), that believe recurrent strain injuries likely occur near these regions of scarring, where the normal contractility mechanics are likely impaired.

The extent of the observed morphological changes showed large variations across subjects. Qualitative assessment of the MR images was able to identify morphological changes that agreed with quantitative measures for 11 of the 14 subjects, with manual segmentation techniques detecting more subtle differences in overall muscle and tendon morphology. A prior study that investigated the reliability of MR imaging and clinical assessment with regards to the evaluation of acute hamstring strain injuries (Schneider-Kolsky et al., 2006). It was found that in 18 of the 58 cases studied, a clinical diagnosis of hamstring injury was made with no positive identification of injury on MR images (Schneider-Kolsky et al., 2006). As a result, it should be expected that a large variation in the extent of remodeling would be present on long-term MR images, as we indeed observed in this study. Because we did not obtain MR images at the time of injury, we cannot definitively prove that the observed differences between limbs are a direct result of a hamstring injury. However, given the similarity of our long-term findings to those observed shortly after original injuries (Connell et al., 2004), we believe it is likely that the differences observed in our study are attributable to the initial hamstring injury. Our observation that asymmetries in morphology between limbs in the control subjects were

much smaller than those observed in the previously injured subjects lends further credence to this conclusion.

The morphological changes that take place following injury may be influenced by a number of factors, including severity of the initial injury, the rehabilitation exercises employed, and the frequency and intensity of training upon return to sport. For example, the hypertrophy present in the short head of the biceps femoris may be an exercise-induced compensation for atrophy of the injured long head. Such a compensation, which is enabled by the separate innervations of the long and short heads, may allow for the preservation of overall knee flexion strength. Periodic MR imaging of individuals from the time of original injury through the return to sport may enable a better understanding of the morphological changes attributable to individual factors during the initial healing process.

All subjects underwent supervised rehabilitation. However, the rehabilitation program was not standardized across subjects. As a result, the observed differences between subjects may be influenced by specific aspects of the rehabilitation strategies employed. Further, the determination of the original injury was performed by a variety of health care providers, as documented in their medical records. Because of this, we cannot report definitively the muscle injured. Additionally, health records could not be obtained for three of the 14 subjects. Thus, the date and location of injury for these subjects was based on direct subject questioning, rather than clinical diagnosis.

Manual segmentation techniques were required to quantify muscle and tendon volumes. Muscle volume estimates obtained from MR image data have previously been

shown to have intra-observer reliability of 4-5% (Tingart et al., 2003; Holzbaur et al., 2007), while accuracy of volume measures estimated from femoral cartilage using 2mm slice thickness resulted in a coefficient of variation for intra-observer variability of 1.2 to 1.3% (Gold et al., 2006). Cartilage volume measures are smaller than hamstring muscle volumes and more comparable to tendon. We conducted an inter-observer reliability test for this study, which resulted in identical agreement in muscle volumes differences between investigators. Discrepancies in tendon volume differences were observed and likely a result of the amount of aponeurosis included in the segmentation process. This was standardized by the investigator that segmented all of the subjects, providing us with confidence in the consistency of the results reported. Manual segmentation takes 10-12 hours to complete for each subject. Thus, an intra-observer reliability analysis was not conducted. Finally, we were unable to accomplish consistent segmentation of the distal hamstring aponeuroses and tendons for volume calculations. This was due to the relatively small thickness of the distal aponeurosis and the intersection of the distal tendon with other low-intensity signal structures that cross the knee.

In conclusion, we have provided evidence of long-term muscle remodeling following a hamstring strain injury. Morphological differences between the limbs of the previously injured subjects were substantially greater than the natural variations occurring in healthy, un-injured athletes. Seventy-nine percent of the previously injured subjects presented with apparent residual scarring at the presumed injury site that persisted a minimum of five months after injury. Of the 13 subjects with biceps femoris injuries, 85% likely returned to sport with residual atrophy of the BFLH and/or

hypertrophy of the BFSH. It is possible that these long-term changes to the musculotendon structure alter the in-vivo contraction mechanics during functional movement, such as running, and may contribute to re-injury risk.

Chapter 2

Identification of Passive Elastic Joint Moment-Angle

Relationships in the Lower Extremity

Introduction

The stretch of soft tissue about a joint generates a passive joint moment that can influence functional movement. Furthermore, the passive elastic moment at one joint is influenced by motion at a neighboring joint due to the stretch of bi-articular muscles such as the rectus femoris, hamstrings, and gastrocnemius. Bi-articulate coupling enables the transfer of energy between joints (Kaya et al., 2005), and is thus important to consider when evaluating the contributions of passive stiffness to gait kinematics and kinetics (Yoon and Mansour, 1982; Mansour and Audu, 1986; Ishikawa et al., 2005).

A double exponential model of passive moment-angle relationships (Davy and Audu, 1987) has previously been used to capture the sharp increase in force that occurs near end-range joint motion. However, the use of exponential models requires accurate kinematic measures since a small deviation in joint angle can cause a large change in the estimated joint moment, and therefore substantially impact the mechanics attributed to passive properties. This factor may contribute to the widely varying estimates of passive contributions to the work and power done during walking (Yoon and Mansour, 1982; Vrahas et al., 1990; Riener and Edrich, 1999). Furthermore, the identification of subject-specific passive moment-angle relationships is often not done, yet is thought to be relevant for understanding the role of passive forces during both normal (Edrich et al.,

2000; McGibbon, 2003; Ishikawa et al., 2005; Muraoka et al., 2005) and abnormal (Cooney et al., 2006) gait. Finally, prior approaches of measuring passive joint moments have only considered a limited number of joint angle combinations (Mansour and Audu, 1986; Vrahas et al., 1990; Edrich et al., 2000) when estimating bi-articular properties, which limits the robustness of the approach.

The purpose of this study was to develop a method for identifying subject-specific passive elastic joint moment-angle relationships about the hip, knee, and ankle, which could then be used to estimate passive contributions to joint kinetics during gait. A key aspect to our approach is the use of the same methodology for measuring joint kinematics in passive and gait analysis, allowing for more consistent estimates of passive joint mechanics than has been achieved previously. We demonstrate this approach by using the identified models to estimate the hip moments arising from the passive stretch of soft tissues during normal walking.

Methods

Experiment: Twenty healthy young adults participated in the study (Table 3). Subjects had no history of major orthopedic diagnosis, musculoskeletal trauma, or persistent joint pain. Each subject gave informed consent according to a protocol approved by the University of Wisconsin's Health Sciences Institutional Review Board.

Table 3. Mean (s.d.) age, mass, and height of the 20 subjects tested.

	Males	Females
Number of subjects	9	11
Age (yrs)	26.1 (4.1)	25.5 (3.1)
Mass (kg)	79.2 (7.6)	59.3 (13.2)
Height (m)	1.82 (0.10)	1.66 (0.10)

The experimental setup (Fig. 6a), was designed to simultaneously measure the joint angles and sagittal plane passive joint moments about the hip, knee, and ankle. Subjects were positioned side-lying with their dominant limb supported on a table via low-friction carts placed under the medial side of the thigh and leg. A padded brace prevented rotation and translation of the pelvis during testing. With the subject relaxed, a physical therapist slowly manipulated the hip, knee, and ankle through full ranges of motion in 15 unique trials using two hand-held three dimensional (3D) load cells (model 45E15A, range 250 lbs; JR3 Inc., Woodland, CA). Load cell forces and moments were recorded at 2000 Hz. The trials were designed to decouple the passive sagittal contributions from the major uni- and bi-articular soft tissues acting about the hip, knee, and ankle joints (Table 4).

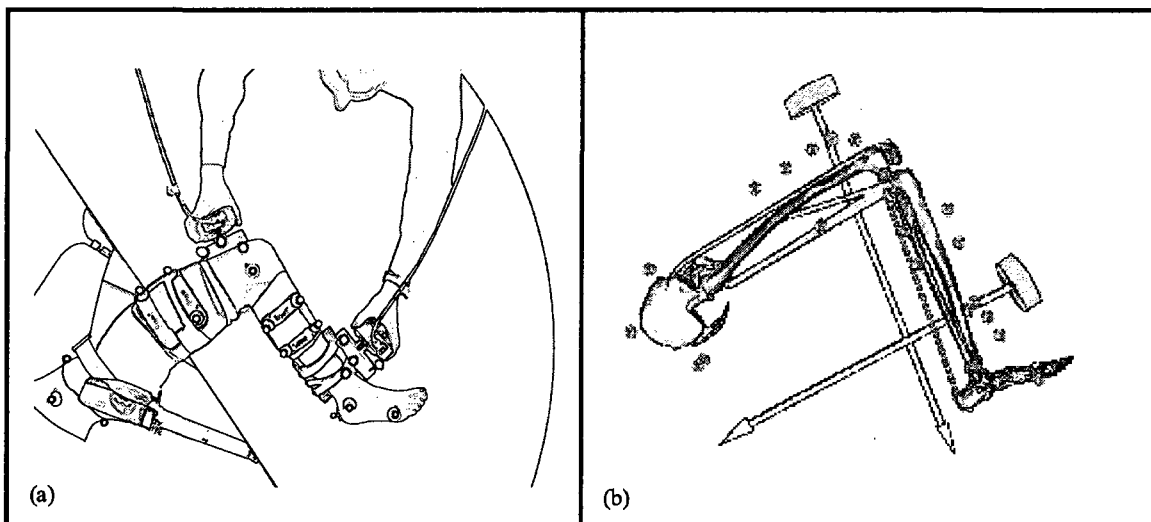


Figure 6: (a) A top view of the apparatus used to simultaneously measure the passive elastic properties of the hip, knee, and ankle. The pelvis was secured to prevent rotation and translation during testing. The positions of reflective markers were monitored to characterize the three-dimensional kinematics of the lower extremity and two hand-held load cells. (b) Measured forces and kinematics were input to a 12 degree of freedom linked segment model to compute the passive moments about the joints of the lower extremity.

Table 2. Fifteen separate trials were used to identify the passive moment-angle relationships. Shown are the approximate joint angles, joint excursions, and the muscles that were stretched. Positive angles represent hip flexion, knee flexion, and ankle dorsiflexion. Negative angles represent hip extension and ankle plantarflexion.

Trial	Hip Flexion (deg)	Knee Flexion (deg)	Ankle Dorsiflexion (deg)	Muscles Stretched
1	-15 – 0	0 – 60	~ -20	RF, HF
2	-15 – 0	0 – 10	~ -20	RF, HF
3	-15 – 0	0 – 135	~ -20	RF, HF
4	0	0 – 135	~ -20	RF, HF
5	0 – 30	0 – 35	~ -20	HAM, HE
6	0 – 30	0 – 135	~ -20	RF, HF, HE
7	0 – 60	0 – 35	~ -20	HAM, HE
8	0 – 60	0 – 135	~ -20	RF, HF, HE
9	0 – 85	0 – 35	~ -20	HAM, HE
10	0 – 85	0 – 135	~ -20	HAM, RF, HE
11	~ 15	0	-20 – 20	GAS, PF
12	~ 15	0 – 60	-20 – 20	GAS, PF
13	~ 15	0 – 135	-20 – 20	GAS, PF
14	-15 – 0	0 – 25	~ -20	HF
15	0 – 100	0 – 25	~ -20	HE

Abbreviations: rectus femoris (RF), hamstrings (HAM), gastrocnemius (GAS), uni-articular ankle plantarflexors (PF), hip extensors (HE), hip flexors (HF), knee extensors (KE), and knee flexors (KF)

Three-dimensional kinematics of the load cells and lower extremity were recorded (100 Hz) using an optical, passive marker motion capture system (Motion Analysis Corporation, Santa Rosa, CA). The position and orientation of each load cell was monitored by four markers rigidly fixed to the load cell frame. Lower extremity motion was tracked via eight markers placed on palpable anatomical landmarks on the pelvis and lower extremity, and an additional seven tracking markers on rigid plates attached to the thigh and shank (Fig. 6). An initial recording using 35 markers was performed with the subject in an upright standing posture to establish bilateral joint centers, body segment

coordinate systems, and segment lengths. In addition, two trials were performed in which the subject circumducted his/her right and left limbs to establish hip joint center locations in the pelvis reference frame (Piazza et al., 2004).

Electromyographic (EMG) signals from seven lower extremity muscles (rectus femoris, vastus lateralis, medial hamstrings, lateral hamstrings, tibialis anterior, soleus, gastrocnemius) were recorded using pre-amplified single differential surface electrodes with a fixed inter-electrode distance of 10mm (DE-2.1, DelSys, Inc, Boston, MA). In preparation for electrode placement, the skin was shaved, cleaned with alcohol, and conductive gel was applied to the electrodes. Muscles of interest were identified, with the same investigator placing the electrodes for all subjects. Electrode and load cell cabling was interfaced to an amplifier/processor unit (CMRR >84 dB at 60 Hz; input impedance > 100 M Ω). Amplification of each channel was adjusted to maximize signal resolution, with EMG data sampled at 2000 Hz using a 12-bit A/D converter interfaced to the collection computer. EMG signals were visually monitored during testing and any trial with detectable muscle activity was repeated.

The pelvis and lower extremity were represented by a 12 degree of freedom (DOF) model (Fig. 6b). The pelvis was the base segment with six DOF. The hip was represented as a spherical joint with three DOF. The knee was represented as a one DOF joint in which non-sagittal rotations and tibiofemoral translations were computed as a function of the knee flexion-extension angle (Walker et al., 1988). The ankle and subtalar joints were represented as pin joints aligned with the anatomical axes (Delp et al., 1990). The dimensions of each segment in the generic model were scaled to individual subjects

such that joint centers and measured marker locations corresponded to virtual locations in the model. At each time step in motion trials, the pelvis position, pelvis orientation, and lower extremity joint angles were computed using an inverse kinematics routine that minimized the sum of squared differences between measured marker positions and corresponding positions of those markers on the model (Lu and O'Connor, 1999). Inverse dynamics analysis was then used to compute the sagittal plane hip, knee, and ankle joint moments from the measured load cell forces and joint angles.

Each subject also performed a series of walking trials at his/her preferred walking speed. Kinematics were recorded using a full body marker set that included, as a subset, the markers used in the passive trials. Ground reaction forces for two successive foot strikes were recorded at 2000 Hz (AMTI, Watertown, MA). Three-dimensional joint angles and joint moments during walking were computed in a manner consistent with the passive testing.

Mathematical Model of Passive Joint Moments: A set of eight exponential functions were developed to account for the stretch of uni-articular structures about the hip, knee, and ankle along with the bi-articular rectus femoris, hamstrings, and gastrocnemius muscles. Uni-articular exponential functions were described by two parameters, gain (β) and offset (α) angle. Bi-articular functions included a third parameter, which ensured the conservation of energy storage and release across joints (see Appendix A). As a result, the predicted passive hip moment (\hat{M}_h) was a function of hip (θ_h) and knee (θ_k) angles. The predicted passive knee moment (\hat{M}_k) was a function

of hip, knee, and ankle (θ_a) angles, and the predicted passive ankle moment (\hat{M}_a) was a function of knee and ankle angles.

$$\begin{bmatrix} \hat{M}_h \\ \hat{M}_k \\ \hat{M}_a \end{bmatrix} = \begin{bmatrix} f(\theta_h, \theta_k) \\ f(\theta_h, \theta_k, \theta_a) \\ f(\theta_k, \theta_a) \end{bmatrix} \quad [1]$$

Model parameters were estimated for each subject by minimizing the sum of squared differences between the measured and predicted passive moments (lsqcurvefit, MATLAB, The Mathworks Inc.). Root mean square (RMS) errors between the measured and predicted passive moments were compared for all subjects and trials. For a subset (n=7) of subjects, the estimated model parameters were used to predict joint moments in eight representative trials not used in the parameter estimation phase. These representative trials traversed a full range of hip, knee, and ankle motion, allowing for an assessment of the validity of the model to represent novel loading scenarios. The passive hip moment during walking was estimated using the joint angles measured during gait as inputs to the passive hip moment-angle function (A.5).

Results

Subject-specific models were able to closely replicate the measured joint moments at the hip, knee, and ankle with average root mean square errors of 2.5 Nm in hip flexion-extension, 1.4 Nm in knee flexion-extension, and 0.7 Nm in ankle plantar-dorsiflexion. These RMS errors did not significantly increase when using subject-specific models to estimate joint moments for the validation trials not used in the parameter estimation phase (Table 5). Within subjects, the repeated trials produced qualitatively similar results (Fig. 7). Between subjects, the gains in the exponential models exhibited

greater similarity across subjects than the offset angles (Table 6). This contributed to more variability in the passive moments at end-range than at mid-range motion (Fig. 8).

Substantial hip flexor moments were estimated when joint angle kinematics during gait were used as inputs to the passive hip moment-angle relationship (A.5). Energy was passively absorbed while the hip was extending from terminal-stance to pre-swing (50-60% of the gait cycle). A peak passive hip flexor moment of ~ 20 Nm occurred just prior to toe-off. Slightly more energy was subsequently returned during pre- and initial-swing (50-73% GC) due to the bi-articular rectus femoris passively transferring energy from the knee to the hip (Fig. 9).

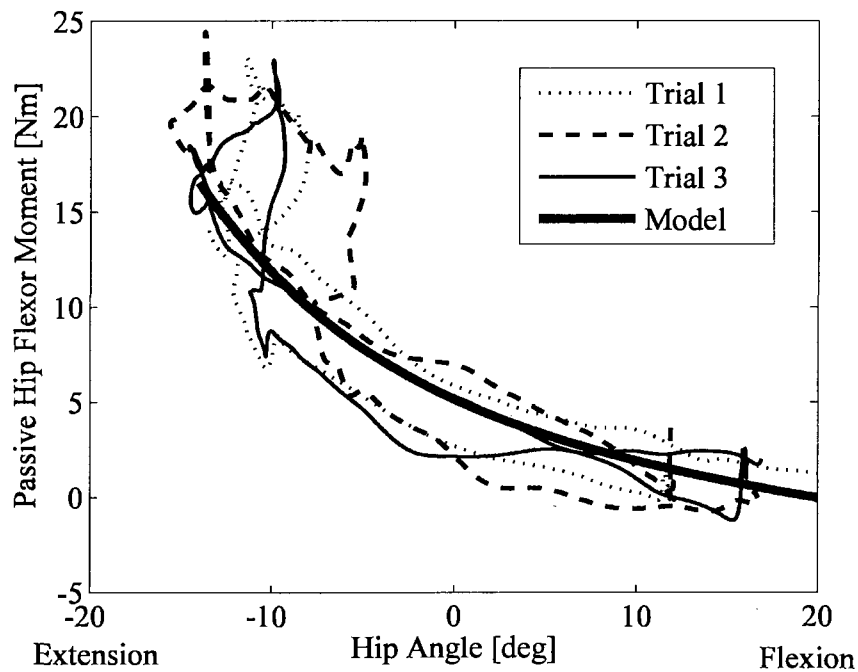


Figure 7: Three representative, repeated trials, in which the hip was first extended and the knee was then flexed. Overlaid is the model-predicted moments using subject-specific parameter estimates. Joint angles from one of the three repeated trials were used as inputs for hip, knee, and ankle angles in the model functions. Both the experimental data and the model contain a loop near full hip extension due to bi-articular rectus femoris stretch as a result of the knee flexion. A slight hysteresis is present in the experimental data, with the moments slightly lower when the hip is flexing than when it is extending.

Table 5. Mean (s.d.) root mean square (RMS) errors between measured and predicted moments (Nm). Subject-specific model parameters were used to predict joint moments in eight additional validations not including in the parameter estimation. Errors between the measured and model predicted moments did not significantly (tested via paired t-tests) vary between the identification and validation trials.

Muscle Function	Gain, β		Offset, α [deg]
	Proximal	Distal	
Rectus Femoris (RF)	3.1 (1.4)	1.9 (0.7)	24.4 (9.0)
Hamstrings (HAM)	5.1 (2.0)	3.9 (2.5)	30.8 (14.9)
Gastrocnemius (GAS)	4.5 (1.6)	4.7 (3.4)	26.0 (28.9)
Hip Flexors (HF)	5.1 (0.9)		19.5 (10.0)
Hip Extensors (HE)	2.0 (0.9)		27.3 (18.0)
Knee Flexors (KF)	5.8 (4.2)		12.8 (13.1)
Knee Extensors (KE)	3.5 (1.7)		101.9 (11.9)
Ankle Plantarflexors (PF)	4.9 (1.5)		-3.4 (5.0)

Table 6. Mean (s.d.) model parameter estimates across the 20 subjects tested.

	Hip	Knee	Ankle
Identification Trials	2.5 (0.5)	1.4 (0.3)	0.7 (0.2)
Validation Trials	2.1 (0.6)	1.2 (0.3)	0.4 (0.1)

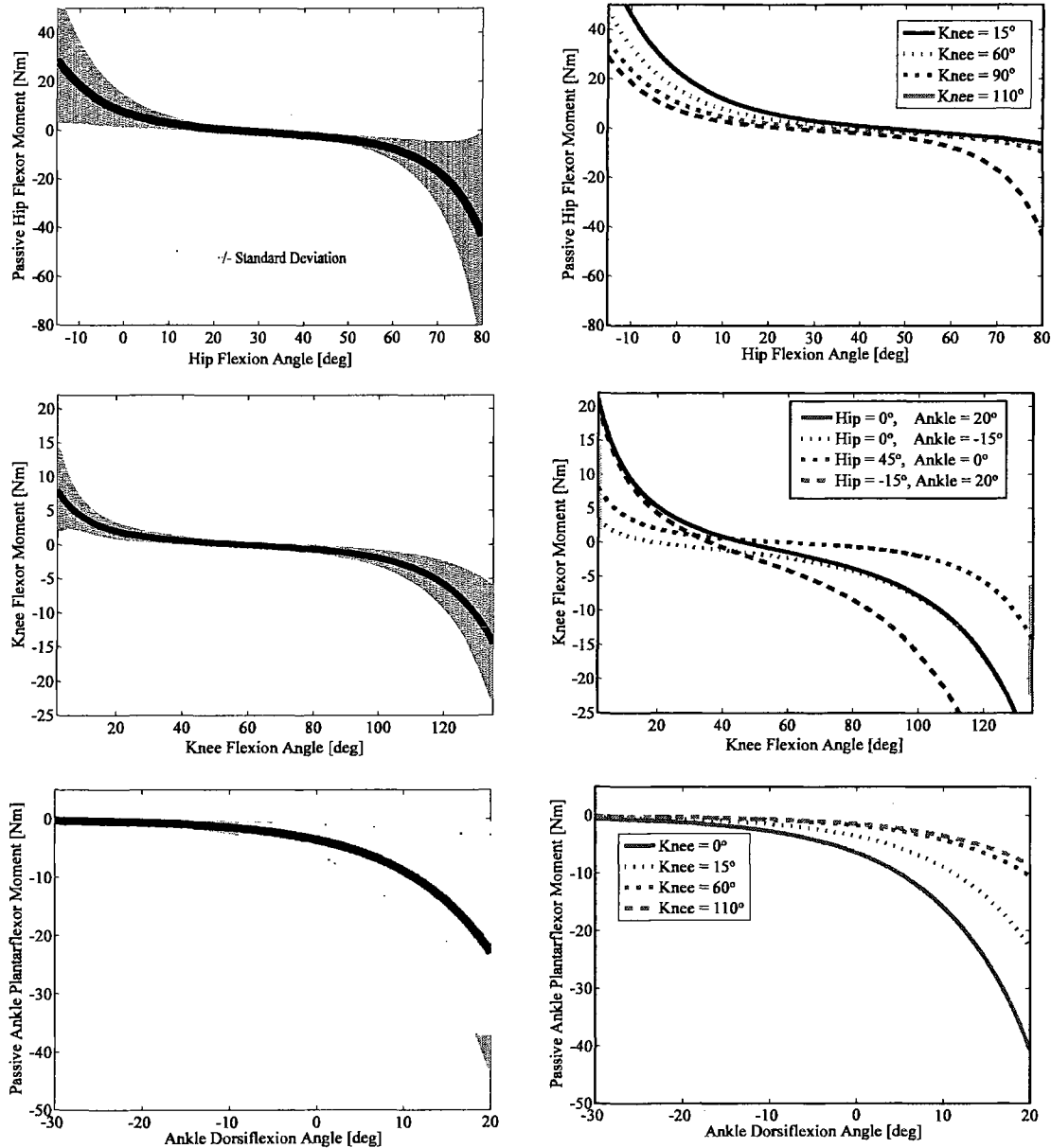


Figure 8: Averaged model predicted joint moment-angle relationships for all 20 subjects. The mean (thick line) and standard deviation (shaded area) were emphasized at representative joint angles (dotted lines) for the hip (knee = 15°), knee (hip = 45°, ankle = 0°), and ankle (knee = 15°). The passive moment changed as the adjacent joint angle(s) varied (dotted lines) demonstrating the contributions of the bi-articular rectus femoris, hamstrings and gastrocnemius.

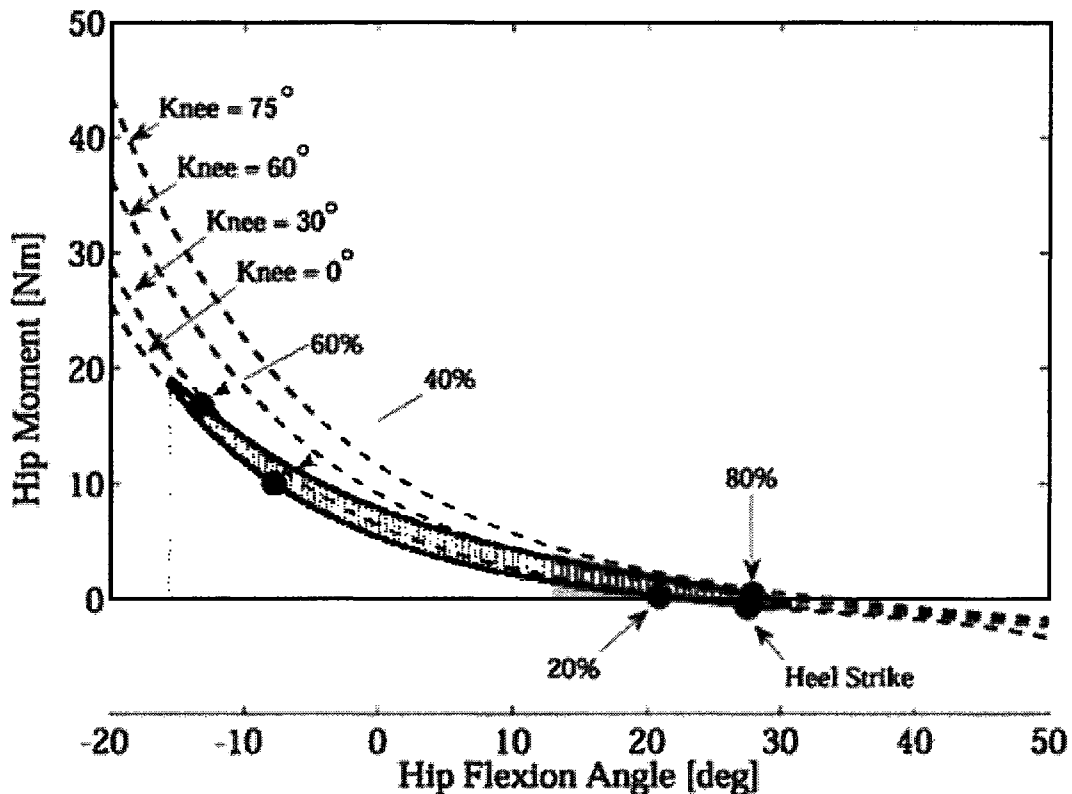


Figure 9: The passive joint moments during walking were estimated by applying the derived moment-angle functions to joint angles measured during walking. The passive hip flexor moment is shown for a single subject at a preferred walking speed. Also shown are the passive hip-flexor moments at 4 fixed knee angles (0° , 30° , 60° , and 75°). Passive energy was absorbed while the hip was extending and returned from approximately pre- to initial-swing (50-73% gait cycle). Slightly greater energy return (cross-hatched area) is achieved via the stretched rectus femoris transferring energy from the knee to the hip.

Discussion

We have introduced a simple experimental setup and mathematical model that can be used to describe the passive joint moment-angle relationships about the hip, knee, and ankle for individual subjects. A unique aspect of our approach was the use of a kinematic marker set that can be directly applied during functional movement, enabling a more consistent description of joint angles and passive moments during movement. This is critical due to the exponential nature of passive forces and the large variability,

particularly at end range motion, that can be introduced due to slight measurement errors in joint angles.

Our model includes the effects of both uni-articular structures (single joint muscles, ligaments, joint capsule, skin) and bi-articular muscles. Other researchers have also shown the need to account for the contribution of bi-articular muscle stretch to passive moments (Mansour and Audu, 1986; Riener and Edrich, 1999; Edrich et al., 2000). However, previous models have not been formulated in a consistent manner that ensures the conservation of energy, i.e. that the energy stored via stretch of a bi-articular muscle is equal to the energy returned by that muscle when it shortens. Enforcing this requirement results in a three parameter model for bi-articular components, rather than a four parameter model that would result from coupling two uni-articular components together (see Appendix A). Our formulation allows for bi-articular muscles to absorb energy via stretch at one joint and then release that energy via shortening at the neighboring joint, as has been observed experimentally (Ishikawa et al., 2005; Kaya et al., 2005).

The simultaneous identification of passive properties about three joints requires that passive measurements be collected over a full range of motion that decouples the contribution of individual components. Our setup was therefore designed to allow each joint to be passively manipulated in the sagittal plane using hand held load cells. The use of motion capture enabled us to monitor three-dimensional joint angles continuously throughout the trials (Table 6). Previous investigators have relied upon the use of a discrete number of joint angles (Mansour and Audu, 1986; Vrahas et al., 1990; Edrich et

al., 2000) to elicit bi-articular responses, as well as ensemble averaged passive joint moments across subjects to estimate parameters (Edrich, et al., 2000; Mansour and Audu, 1986; Riener and Edrich, 1999; Yoon and Mansour, 1982). Such simplifications could limit the resolution with which passive properties can be identified. It should be noted that in our approach, the use of data from a subset of trials could be used if one is only interested in select muscles. For example, we have been able to obtain reasonable estimates of the parameters of the hamstrings in healthy subjects by including only those trials that involve substantial hip and knee extension.

A limitation of the proposed mathematical model is that it does not account for a slight hysteresis present in the passive moment-angle data (Fig. 7). Our parameter estimation includes both the increasing and decreasing parts of the moment-angle curve, thereby splitting the difference in the fit. This compromise likely results in a slight under-estimation of the peak passive moment and an over-estimation of the passive energy returned. Identifying the parameters of a model that includes viscoelastic effects is much more challenging since this would also require manipulation of the joint velocity (Yoon and Mansour, 1982; Vrahas et al., 1990).

Others (Vrahas et al., 1990; Edrich et al., 2000) have demonstrated relatively small between-trial variability in passive joint moments as we observed (Fig. 7). Due to the length of our entire testing procedure, we did not repeat the entire set of calibration trials necessary to re-estimate the model parameters. However, we did use the identified models to estimate moments during unique trials not using in the model fitting, and found good agreement between the measured and predicted moments.

A potential source of error in our procedure arises from the calculation of joint angles and joint centers from skin-mounted markers. We minimized these errors by taking extra care that the markers remained fixed between the upright calibration trials and the side-lying testing procedures. We also employed a functional hip joint center identification method, which has been shown to reduce errors in locating the hip joint center (Piazza et al., 2004). However, it remains possible that errors in the estimate of the hip joint center location led to the larger errors in passive moments at the hip compared to the knee and ankle (Table 5).

Electrical activity in select muscles was monitored to ensure a truly passive test. We occasionally observed some reflex activity, for example in the tibialis anterior during dorsiflexion trials. In these cases, the trials were repeated and all of our subjects were capable of eliminating the activity levels upon repeat testing. However the suppression of reflex activities may be challenging for individuals with neuromuscular impairments, in which case it may be necessary to account for active responses superimposed on the passive measures. In addition, muscle activities were recorded on only seven selected superficial muscles so the relaxed state of other muscles, e.g. deeper muscles like the iliopsoas, could not be directly confirmed.

In using the passive moment-angle relationships to estimate passive contributions during movement such as gait, one inherently assumes that the passive properties are additive with the active components present. This is likely a reasonable assumption for fully passive structures such as the joint capsule, ligaments, and skin. However, the interaction of passive and active components in muscle remains an area of active research

(Epstein and Herzog, 2003), making it more challenging to quantify precisely how passive components are utilized in movement. Furthermore, our methodology only considered the influence of sagittal plane passive joint moments, which may be reasonable in normal gait. However, further investigation is needed to apply these techniques to pathological gait, e.g. cerebral palsy or stroke, where non-sagittal motion may be considerable.

Applying the passive moment-angle curves to gait demonstrates the potential for substantial contribution of both passive uni- and bi-articular muscle stretch to the joint moments observed (Fig. 9). Our results suggest that passive mechanisms may contribute substantially to the hip flexor moment seen during normal gait. Hip flexor moments are estimated to reach ~50 Nm during normal adult walking (Kerrigan et al., 1998). We estimated a passive moment of ~20 Nm, meaning that nearly one-half of the hip flexor moment may arise from passive structures. Others have estimated the passive hip flexor moments at toe-off as between 10-50% (Yoon and Mansour, 1982; Vrahas et al., 1990) of the net component, putting our estimate near the upper end of this range. This moment occurs due to the passive stretch of the uni-articular hip flexors and bi-articular rectus femoris, enabling the absorption of energy during terminal stance and passive return during pre- and initial-swing. The ability of passive structures to store and release energy during normal gait may substantially reduce the active generation of energy required to initiate swing and generate propulsion.

Our methodology could be used to investigate the role that impairments play in abnormal gait. For example, it has been suggested that hip flexion contractures may be

used by impaired elderly to passively assist the initiation of limb swing motion (McGibbon, 2003). In addition, it is thought that passive forces arising from tight hamstrings may contribute to diminished terminal swing knee extension commonly seen in children with cerebral palsy (Cooney et al., 2006). Quantifying the contributions of passive properties to the joint moments and powers observed during abnormal gait may provide new insights into the biomechanical function of impairments during walking.

Chapter 3

Influence of a Prior Hamstring Strain Injury on Strength, Flexibility, and Biomechanical Function

Introduction

Hamstring strain injuries are extremely common in sports that involve sprinting, such as track, soccer, baseball/softball, and football (Kujala et al., 1997; Jarvinen et al., 2000; Arnason et al., 2004). However, the effective treatment and rehabilitation of individuals with hamstring injuries remains a challenge, as demonstrated by a re-injury rate of approximately 30% (Orchard and Best, 2002; Woods et al., 2004). A number of different rehabilitation strategies have been proposed for reducing re-injury risk with varying degrees of emphasis placed on hamstring stretching (Agre, 1985), strengthening (Agre, 1985), eccentric exercises (Proske et al., 2004), and/or trunk stabilization exercises (Sherry and Best, 2004). Regardless of the rehabilitation program employed, it continues to be extremely challenging for a clinician to assess when an athlete can safely return to sport. Previous studies have found that physical exam findings at the time of injury (Tuite and DeSmet, 1994; Warren et al., 2008) or end of rehabilitation (Sherry and Best, 2004) are relatively ineffective at predicting injury recurrence. Hence, a better understanding of the effects of a prior injury on hamstring mechanics and function could provide a basis for establishing more quantitative return to sport criteria.

The majority of hamstring injuries that occur during sprinting involve the proximal musculotendon junction of the biceps femoris long head (BFLH) (Orchard and Best, 2002; Askling et al., 2007; Silder et al., 2008). Following a strain injury, muscle tissue is likely unable to fully regenerate to its pre-injury state. In particular, imaging studies have found evidence of scar tissue as soon as 6-weeks post injury (Connell et al., 2004), and animal models have shown that such scarring persists indefinitely (Kaariainen et al., 2000; Best et al., 2001). In a recent study, we presented evidence of scar tissue adjacent to the site of prior hamstring injuries many months following initial injury (Silder et al., 2008). It is likely that this injury induced change in morphology alters in-vivo musculotendon mechanics. For example, Brockett et al. (Brockett et al., 2004) found that athletes who sustained a previous unilateral hamstring injury developed peak knee flexion torque at a greater knee flexion angle (i.e., shorter muscle length), when compared to the uninjured limb. Such a shift could reflect the presence of scar tissue, which may reduce the effective length of the muscle tissue and may also contribute to greater passive stiffness of the musculotendon unit. The replacement of contractile tissue with connective scar tissue could alter lateral force transmission paths, reduce the length of adjacent muscle fibers, and influence both the passive and active force-length properties of the musculotendon unit. It is not yet known whether athletes also adapt their running patterns in a way that allows the previously injured hamstrings to operate at shorter lengths.

Several authors have suggested injury risk may be influenced by hamstring weakness and/or a hamstrings/quadriceps muscle imbalance (Agre, 1985; Clark, 2008).

However, there is insufficient evidence to definitively conclude that a relative weakness or imbalance may be a risk factor for re-injury. Some studies have reported strength deficits in athletes with a history of recurrent strains (Jonhagen et al., 1994; Croisier et al., 2002), while other studies have reported normal strength after injury (Paton et al., 1989; Worrell et al., 1991). For individuals with prior injury to the proximal biceps femoris (BF), we previously observed significant atrophy of the BFLH and corresponding hypertrophy of the biceps femoris short head (BFSH) (Silder et al., 2008). It is possible that such morphological changes represent a compensatory mechanism to maintain knee flexion strength. In addition to changes in morphology of neighboring muscles, it is feasible that athletes may modify neuromuscular coordination and movement patterns in a way that alters the biomechanical demands placed on the previously injured muscle.

The purpose of this study was to determine if bilateral differences in isokinetic strength characteristics, passive hamstring stiffness, as well as kinematics and neuromuscular control during treadmill sprinting exist in individuals with a prior hamstring strain injury. These measures were also compared to the musculotendon morphology data previously reported for these same individuals (Silder et al., 2008). The overall hypothesis was that the degree of post-injury remodeling would reduce optimal hamstring lengths for force generation, increase passive musculotendon stiffness, and induce functional compensations that reduce hamstring stretch during sprinting.

Table 6. Demographics and information regarding the prior injury/injuries of the subjects participating in this study. *Subjects did not participate in sprinting protocol. Abbreviations: SM = semimembranosus; BF = biceps femoris, ST = semitendinosus.

Subject	Gender	Age	Months from Injury	Side of Injury	Location of Injury	Number of Injuries	Activity at Time of Injury
1	Male	18	5	Right	Proximal BF	1	Soccer
2	Male	38	5	Left (recent) Right (prior)	Distal ST (recent) Proximal BF (prior)	2	Soccer
3	Female	17	5	Right (both)	Distal BF (both)	2	Track (sprinting)
4	Male	31	5	Left (both)	Proximal BF (both)	2	Football (sprinting)
5	Male	23	5	Right (both)	Distal BF (recent) Proximal BF (prior)	2	Track (sprinting)
6	Male	19	13	Left (both)	Proximal BF (both)	2	Track (sprinting)
7	Female	19	7	Left (both)	Proximal BF (both)	2	Track (hurdling)
8	Male	18	8	Right (all)	Proximal BF (all)	3	Track (sprinting)
9*	Female	43	9	Right (both)	Proximal BF (both)	2	Softball
10*	Male	20	7	Right	Distal BF	1	Track (sprinting)
11*	Female	45	6	Right	Distal BF	1	10k race

Materials and Methods

We tested eleven athletes who had experienced a hamstring strain (grade I or II) between 5-13 months prior (Table 6). All subjects were involved in running related sports, participated in a supervised rehabilitation program for a minimum of two weeks, and had since returned to full sporting participation. Exclusion criteria included complete hamstring muscle disruption (grade III) or avulsion, current other lower extremity injury, history of hip or knee joint surgery, lower extremity nerve entrapment, and presence of lower extremity or back pain with running. Each subject or parent provided written informed consent prior to testing, in accordance with the University of Wisconsin's Health Sciences Human Subjects' Committee. The testing protocol included four parts: magnetic resonance (MR) imaging, isokinetic knee flexion/extension strength testing, passive joint stiffness testing, and a biomechanical assessment of treadmill sprinting.

MR Imaging Protocol: MR images of the injured and un-injured limbs were obtained for each subject on a 1.5 Tesla Twin Speed magnetic resonance scanner (General Electric Healthcare, Milwaukee, Wisconsin). Bilateral comparisons of the images were used to evaluate the presence mature scar tissue, which appears as low intensity signal (Tuite and DeSmet, 1994; Best et al., 2001). Images were also used to quantify the relative volume of tendon/scar and muscle tissue for the BFLH and BFSH in both limbs. Details of the imaging protocol, analysis, and complete results can be found elsewhere (Silder et al., 2008).

Strength Testing: Subjects were positioned on an isokinetic dynamometer (Biodex Multi-Joint System 2, Biodex Medical Systems, Inc.) such that the hip was flexed to 90

deg and the dynamometer and knee joint axes were aligned. Strapping was used over the shank, thigh, and waist to minimize secondary joint movement. Each subject performed five consecutive isokinetic (60 deg/s) knee flexion/extension cycles through their available range of motion and were verbally encouraged to perform at maximum effort. Joint angle and torque were recorded, and torque measurements were corrected for gravity. For each strength test, we determined the cycle in which peak knee flexion torque was generated, and then extracted the corresponding angle of peak torque. We similarly determined the peak knee extension torque, and used that to quantify the hamstrings to quadriceps peak torque ratio.

Biomechanical Assessment of Treadmill Sprinting: Eight of the eleven subjects performed treadmill running at 60, 80, 90, and 100% of maximum sprinting speed. Whole body kinematics were recorded using an eight-camera passive marker system (Motion Analysis Corporation, Santa Rosa, CA). Thirty reflective markers were placed on palpable anatomical landmarks, while 18 markers were placed on body segments to improve the model fit to the experimental data. A calibration trial was first performed to establish joint centers, body segment coordinate systems, segment lengths and the local positions of tracking markers. A functional hip joint center algorithm was implemented (Piazza et al., 2004) to estimate the location of a ball-and-socket representation of the hip in the pelvis reference frame. Marker kinematics recorded during the running trials were used to compute three-dimensional lower extremity joint angles. These data were then used together with a scaled lower extremity musculoskeletal model (Delp et al., 1990; Hoy et al., 1990) to estimate bilateral hamstring muscle lengths throughout the running

gait cycle. Software to perform the kinematic analyses were generated using SIMM Dynamics Pipeline (Motion Analysis; Santa Rosa, CA) and SDFast (Parametric Technology Corp.; Needham, MA). Bilateral peak hip, knee, and ankle angles, along with peak BF musculotendon lengths were found for all strides (~5 strides) and for each speed. After determining no significant variations existed in joint angles or musculotendon lengths between strides, we then used the mean values to assess potential asymmetries in running mechanics.

EMG measurement: Bilateral muscle activities of the rectus femoris (RF), vastus lateralis (VL), BF, and medial hamstrings (MH) were recorded at 2000 Hz using pre-amplified single differential electrodes (DE-2.1, DelSys, Inc, Boston, MA). In preparation for electrode placement, subjects' skin was shaved and cleaned with alcohol. The electrodes were coated with conducting gel prior to application and interfaced with an amplifier/processor unit (CMRR > 85 dB at 60 Hz; input impedance > 100 M Ω). The electrode locations were determined by the same investigator for each subject using standard EMG electrode locations (Basmajian, 1985). EMG signals were first passed through a 20–500 Hz, sixth order Butterworth filter and then full wave rectified. Each EMG signal was normalized to the mean EMG signal of that muscle over an entire gait cycle from the 100% sprinting speed. The onset, offset, and duration of muscle activity, relative to a gait cycle, was manually determined. (Li and Aruin, 2005) Magnitude of normalized EMG activity was assessed by finding the mean signal during four distinct phases of the gait cycle: loading, propulsion, initial swing, and terminal swing. These phases were divided by the instantaneous events of initial contact, stance phase reversal,

toe-off, and swing phase reversal, where stance phase and swing phase reversal were each defined as the transition from knee flexion to extension (Ounpuu, 1990; Novacheck, 1998).

Passive Joint Stiffness: Each subject who participated in the sprinting protocol also underwent passive joint stiffness testing. Subjects were positioned side-lying with their limb placed on a table and supported via low-friction carts. With the subject relaxed, a physical therapist (BH) slowly manipulated the hip and knee angles using two hand-held three dimensional (3D) load cells (Model 45E15A, JR3 Inc., Woodland, CA). Limb kinematics were simultaneously recorded with the load cell data, and then used to compute the passive hip extension torque and sagittal hip and knee angles throughout a series of 14 unique trials. These data were used to identify subject-specific passive hip moment-angle models for each limb. The model and experimental protocol were designed to decouple the contributions of the uni-articular hip extensors and bi-articular hamstrings (Silder et al., 2007). The model parameters for each subject-limb combination, along with hip and knee angles, were used as inputs into the model. This resulted in the passive hip flexor moment at each corresponding combination of joint angles (Fig. 10). Passive hamstring stiffness was defined as the hip flexion angle at which the passive hip flexor moment reached -30 Nm.

Statistical Analyses: All bilateral differences are reported as percent difference relative to the un-injured limb. Strength testing and passive joint stiffness testing measures were compared using paired t-tests ($\alpha=0.05$), while sprinting measures were compared using repeated measures ANOVA. The following strength testing measures

were compared: peak torque, angle of peak torque, and hamstring/quadriceps peak torque ratio. We assessed bilateral differences during sprinting for peak joint angles, BF musculotendon lengths, normalized mean muscle activities, and muscle activation timing. The relationship between morphology (i.e. muscle and tendon/scar volumes) and biomechanical measures were assessed by first ranking the subjects in order of the extent of remodeling present. Comparisons were then made between the degree of remodeling present and the degree of bilateral asymmetries measured in the current study.

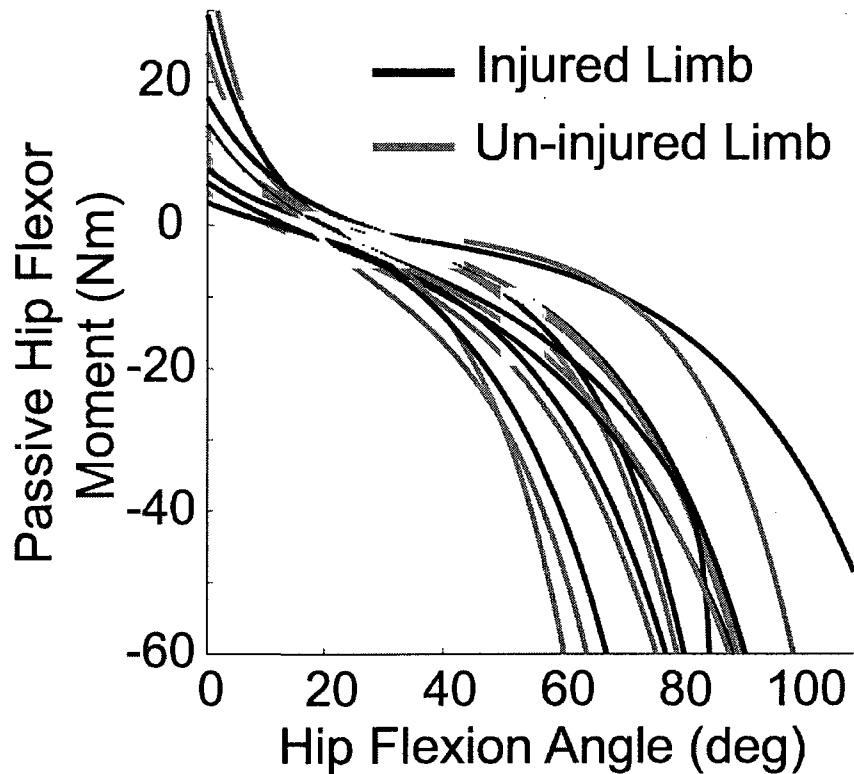


Figure 10: Model predicted passive hip flexor moments for each subject and limb that participated in the sprinting protocol. Variability in joint stiffness was apparent across individuals. Due to the bi-articular rectus femoris and hamstrings, passive hip joint stiffness is dependent on both hip and knee angles. For this analysis, the knee angle was fixed at zero degrees of flexion, while the hip angle was varied between 0-110 degrees of flexion.

Table 7: The table represents differences between the injured and un-injured limbs. Percent change in muscle and tendon volumes between the injured and non-injured limbs was adapted from (Silder et al., 2008). The subjects were organized according to the degree of scarring present. Negative values in muscle/tendon volume indicate the injured limb to be smaller than the non-injured limb. Peak isokinetic torque measures revealed no deficits in strength. Angle of peak torque measures were used to assess any changes in long term active force length relationship of the muscle. A positive value for angle of peak torque indicates that peak torque was produced at a more flexed knee angle for the injured limb. Similarly, positive values for the peak torque and the hamstring/quadriceps peak torque ratio indicate that this value was larger for the injured limb. A positive value for hamstring stiffness indicates the injured limb to be stiffer, while a positive value for peak biceps femoris musculotendon stretch during sprinting indicates a greater overall stretch of the injured musculotendon unit during sprinting. Abbreviations: BFLH = biceps femoris long head muscle; BFSH = biceps femoris short head muscle; BFT = combined proximal biceps femoris and semitendinosus tendon; Ham = hamstrings; Quad = quadriceps.

Subject	Muscle/Tendon Volume			Peak Torque (%)	Angle of Peak Torque (deg)	Ham/Quad Ratio (%)	Hamstring Stiffness (deg)	Peak Hamstring Stretch (%)
	BFLH	BFSH	Proximal BFT					
1	-4	23	218	13	-9	-11	2	0.10
5	-1	-1	132	45	7	54	5	0.33
6	-12	17	124	-3	14	1	1	0.68
4	-23	1	114	-7	16	-7	3	0.42
7	-16	46	105	-24	21	-18	-1	0.23
11	-26	25	11	6	-5	56	---	---
3	-6	9	10	-38	0	-42	10	-0.69
9	-20	30	0	-33	-6	-56	---	---
2	3	-21	-4	36	5	55	2	-0.22
10	-4	-3	-6	30	-15	29	---	---
8	5	16	-7	24	1	4	18	-0.03

Results

Clinical notes indicated that all eleven subjects sustained injuries to the BF on one or more occasions. Eight subjects sustained at least one re-injury, with six of these re-injuries occurring in the same region (i.e. proximal or distal) and muscle (Table 6).

When considering all the subjects tested, no significant bilateral differences were observed in peak knee flexion torque, angle of peak torque, or the hamstrings/quadriceps peak torque ratio (Table 7). However, after sorting the subjects according to the degree of scarring, greater consistency did emerge in the angle of peak torque. In particular, the angle of peak torque was shifted to a more flexed knee on the injured limb in four of the five subjects with the largest amount of scarring (e.g. subjects 1,4,5,6,7). The average bilateral difference for these five subjects was 10 deg, compared to a -3 deg difference for the remaining six subjects. The degree of BFLH atrophy and/or BFSH hypertrophy did not consistently relate to any of the strength testing measures obtained.

Passive hip joint stiffness was more variable between subjects than between limbs (Fig 10). Small differences were observed in joint stiffness between the injured and uninjured limbs for most subjects. However, these differences were not consistent and did not seem related to morphological measures previously obtained (Table 7).

Some individuals showed bilateral asymmetries in kinematic measures during running. However, these differences did not consistently relate to the injured limb, and no significant differences were observed in peak joint angles between limbs. Correspondingly, peak BF musculotendon lengths were not significantly different between limbs (Table 7) and the ensemble averaged curves for both limbs across the gait

cycle were nearly indistinguishable (Fig. 11). There were no significant differences in the magnitudes of hamstring activity between limbs for any of the four phases. However significant differences between limbs were observed for the VL during loading at 80% and 90% speed, the VL during propulsion at 60% speed, and the RF during loading at 90% speed. In each of these cases, quadriceps activity was significantly higher in the un-injured limb. Irrespective to the side of injury, the greatest hamstring activity occurred during terminal swing and initial stance (Fig. 12). However, there were no significant differences in the onset, offset or duration of muscle activities between the injured and un-injured limb across any of the four speeds (Fig. 13).

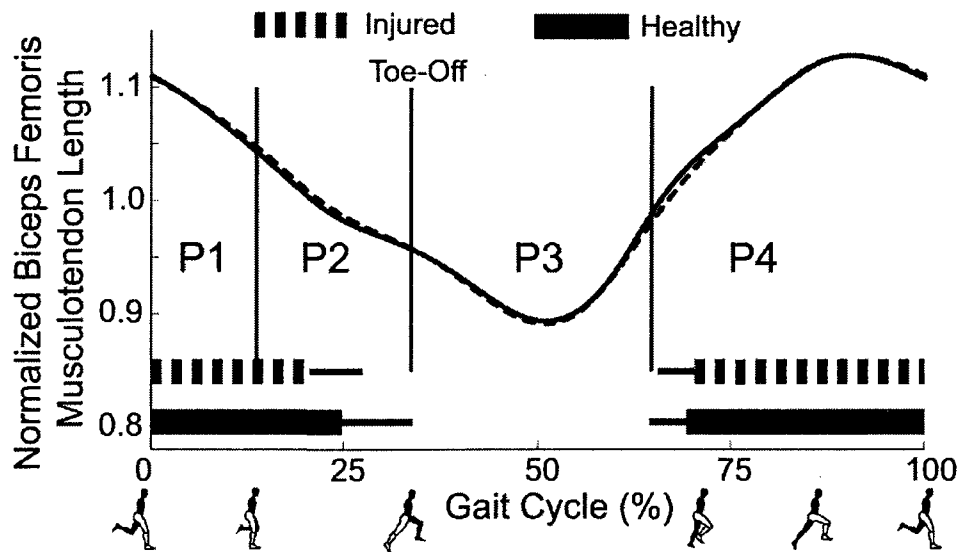


Figure 11: The ensemble averaged biceps femoris musculotendon lengths normalized to upright standing posture were nearly identical between the injured and un-injured limbs during sprinting (100% speed shown). The thick horizontal lines (standard deviation, thin line) represent when the biceps femoris muscle was active during the gait cycle. Slight differences were observed in the timing of muscle activity between the injured and un-injured limb. However, these differences were not significant. Abbreviations: P1, loading; P2, propulsion; P3, initial swing; P4, terminal swing.

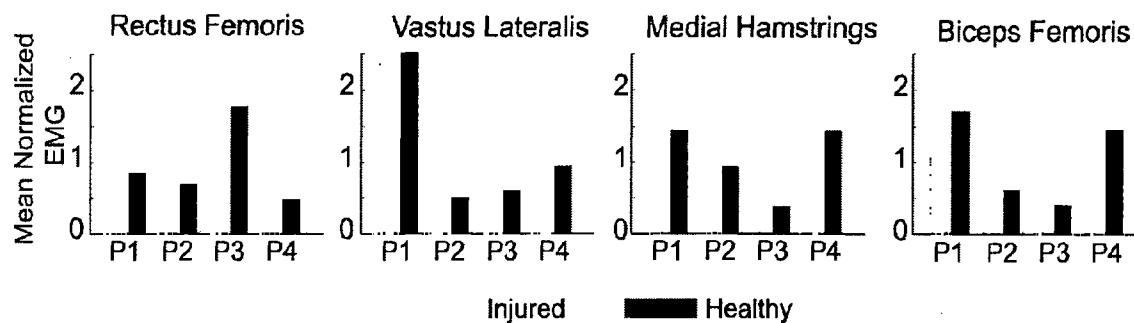


Figure 12: Mean ensemble averaged EMG values were calculated for each phase of the gait cycle (100% shown). No significant differences were observed between limbs at any of the sprinting speeds tested. The hamstrings are most active during terminal swing and loading, when they act to decelerate the limb prior to foot contact and advance the center of mass forward, respectively. Abbreviations: P1, loading; P2, propulsion; P3, initial swing; P4, terminal swing.

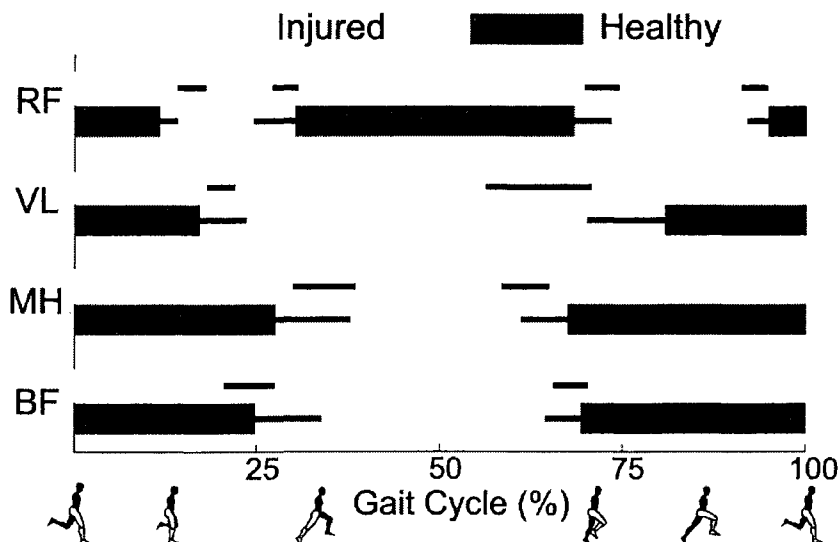


Figure 13: Ensemble averaged muscle activation timing was similar between the injured and un-injured limbs for all speeds (100% speed shown). Slight differences between limbs were observed for individual subjects, but were not consistent or significant. Abbreviations: RF, rectus femoris; VL, vastus lateralis; MH, medial hamstrings; BF, biceps femoris

Discussion

The goal of this study was to investigate how post-injury remodeling following a hamstring strain injury might affect both the mechanics and function of the musculotendon unit. In a prior study (Silder et al., 2008), we used MR imaging to qualitatively and quantitatively describes the long-term changes in the muscle and tendon morphology for these same individuals. We found a significant degree of scar tissue along the musculotendon junction adjacent to the site of prior injury. In addition, atrophy of the BFLH was present on the side of injury and was often accompanied by hypertrophy of the BFSH. These significant changes led us to hypothesize that functional adaptations would also be detectable in these individuals. The results of the current study suggest that morphological changes resulting from prior injury may induce a shift in the muscle's optimal operating range. However, these effects were not consistently discernable from joint stiffness measures, EMG, or biomechanical assessments of running.

We hypothesized that the replacement of muscle with scar tissue following injury could reduce the optimum length for active force generation. Such a change would be detectable at the joint level in terms of peak knee flexion torque occurring at a more flexed knee angle. While we did not observe a significantly consistent shift in angle of peak torque across all subjects, the five subjects with the largest amount of scarring did indeed exhibit a 10 deg (43%) increase in the angle of peak torque compared to the uninjured limb. Brockett and colleagues (Brockett et al., 2004) tested a group of previously injured athletes from the Australian Football League and found that peak torque in the

previously injured limb occurred at a greater knee flexion angle (12 deg more) than the contralateral limb. They had speculated that the change could be attributable to post-injury musculotendon remodeling or alternatively may be a training effect resulting from the repeat performance of concentric strengthening exercises during rehabilitation. Our results would support the former explanation, and would suggest that interventions aimed at reducing the presence of scar tissue may minimize this change in strength properties.

We quantitatively assessed running mechanics to ascertain how injury induced changes at the muscle level might be evidenced in running. Hamstring strain injuries are generally believed to occur during late swing (Woodley and Mercer, ; Wood, 1987), During this time, the hamstrings undergo a lengthening contraction, with a reversal to shortening just prior to foot contact (Fig. 11). This suggests that the hamstrings are likely absorbing substantial amounts of energy during this phase, and would seem susceptible to a lengthening contraction injury. Hence, a protective mechanism may involve adapting running mechanics in such a way that reduces the stretch and energy absorption of the previously injured hamstrings. We did not measure external forces and thus were unable to estimate the loads and energy absorbed by the hamstrings. However at the kinematic level, there were no significant asymmetries detected in peak hip flexion, knee extension or hamstring musculotendon stretch at any of the speeds (Fig. 11). All of our sprint testing was done in a non-fatigued state with data collected for ~5 strides per speed. It has been previously shown that repeated tests at maximal sprinting effort can cause significant changes in running technique (Pinniger et al., 2000), such that asymmetries may arise with fatigue.

We measured EMG activities during running to assess whether coordination may be adapted to protect the previously injured hamstrings. While individual subjects exhibited some asymmetries in the timing and magnitude of hamstring activities, no consistent trends emerged. Interestingly, we did identify some significant differences in quadriceps activity, with subjects exhibiting greater activation in the VL and RF on their un-injured limb during loading at sub-maximal sprinting speeds. Quadriceps activity during this phase is used to stiffen the limb, and absorb impact loads. However, since the net ground reaction force is directed posteriorly, the net effect of limb loading during this phase contributes to breaking forward propulsion. It has previously been speculated that hamstring activity during late swing acts reduce the forward braking during loading (Mann, 1981). It is unclear whether a reduction in quadriceps activity in the previously injured limb during loading may represent an adaptation that alters the use of the previously injured hamstring or is an underlying neuromuscular coordination factor associated with injury risk. Thus, the use of an instrumented treadmill to assess joint and muscle kinetics in conjunction with EMG analysis during running is needed to investigate such potential mechanisms in more detail.

There are some limitations to consider when interpreting the results of this study. Notably while all subjects underwent supervised rehabilitation, the rehabilitation program itself was not standardized across subjects. As a result, the observed differences between subjects may be influenced by specific aspects of the rehabilitation strategies employed. For example, we hypothesized that the presence of scar tissue would increase the passive stiffness of the muscle-tendon unit (Brockett et al., 2004). Small differences were

measured in the overall joint stiffness between limbs (Fig. 10). However, these differences were not consistent and did not appear to be associated with the degree of scarring resulting from injury (Table 7). These, as well as asymmetries during running and strength testing may be further influenced by a number of factors including limb dominance, severity of the initial injury, and the frequency and intensity of training upon return to sport. For example, the hypertrophy present in the BFSH may be an exercise-induced compensation for atrophy of the injured long head. Such a compensation, which is enabled by the separate innervations of the long and short heads, may allow for the preservation of overall knee flexion strength and may help to explain the similar peak knee flexion torque observed in this, and other studies (Croisier, 2004).

The vast majority of hamstring muscle tears occur at or near the musculotendinous junction of the proximal BF (Garrett et al., 1989; De Smet and Best, 2000; Koulouris and Connell, 2003). All 11 of the subjects in this study sustained injuries to the BF, with eight of those injuries occurring along the proximal musculotendon junction. As a result of the change in mechanical properties due to the scar tissue, local tissue strains may be increased during times of high external loads (Silder and Thelen, 2009). Some rehabilitation programs have been designed to limit the residual adverse effects of scar tissue formed during the remodeling process (Kujala et al., 1997; Jarvinen et al., 2000; Kaariainen et al., 2000). The incorporation of more advanced dynamic MR imaging techniques (Asakawa et al., 2006; Silder and Thelen, 2009) or ultrasound may lend more focused insights into the functional affects of scar tissue on local tissue mechanics. Such approaches could provide a more quantitative means for understanding

injury effects, and for establishing evidence-based rehabilitation programs that mitigate re-injury risk.

Chapter 4

A MR-Compatible Loading Device for Dynamically Imaging Shortening and Lengthening Muscle Contraction Mechanics

Introduction

Dynamic magnetic resonance (MR) imaging is a powerful approach for characterizing in-vivo muscle mechanics. For example, studies have shown that muscle fascicles and aponeurosis do not shorten uniformly (Pappas et al., 2002; Finni et al., 2003), as commonly assumed in muscle models (Zajac, 1989). More recent techniques have revealed a strong influence of musculotendon architecture on the spatial finite strain distributions within contracting muscle (Zhou and Novotny, 2007; Zhong et al., 2008). Such information can be extremely helpful for improving our understanding of dynamic muscle function, for validating musculoskeletal models, and for critically evaluating the effects of clinical interventions.

MR compatible limb loading devices, capable of inducing elastic loads, have been successfully used during dynamic MR imaging to investigate shortening muscle contraction mechanics (Drace and Pelc, 1994; Pappas et al., 2002; Asakawa et al., 2003; Hidler et al., 2006). However, functional movement often involves active stretch-shortening cycles, during which the musculotendon lengthens under load prior to shortening (Komi, 1984). During the lengthening phase, muscle fibers can undergo an active lengthening contraction, which enhances force development but also makes it more susceptible to injury (Lieber and Friden, 2002). Therefore, understanding in-vivo tissue

motion during lengthening contractions is relevant to understand both normal muscle function, and potential injury mechanisms.

The goal of this study was to develop a MR-compatible device that can be used to impose either elastic or inertial loads on skeletal muscles, thereby inducing either shortening or lengthening contractions. Our initial focus is on the hamstrings, which is one of the most frequently injured muscles among athletes (Noonan and Garrett, 1999) and undergoes a stretch-shortening cycle during the late swing phase of running (Thelen et al., 2006). The primary challenge of this investigation was to generate sufficient inertial loads (proportional to mass*acceleration) within the physical constraints of a scanner and the temporal constraints of dynamic MR pulse sequences. We address this issue by using a geared loading assembly to amplify the effective inertia felt by the hamstrings during cyclic knee flexion-extension. In this paper, we describe the design of the device and confirm that it induces repeatable motion and the intended muscle contractions, which are both crucial for dynamic image acquisition and analysis. Preliminary data obtained from cine phase-contrast (cine-PC) imaging are presented to demonstrate the effectiveness of the device during MR image acquisition.

Methods

Device Description: The device was designed to achieve the following goals: a) guide the limb through repeatable cyclic knee flexion-extension, while limiting thigh movement, b) impose variable inertial or elastic loads on the hamstrings, c) be constructed of non-ferrous materials, resulting in the device being both MR safe and

compatible (Shellock, 2002), and d) fit within the 60cm bore diameter of a standard MR scanner. Following is a detailed description of the components of the device.

Base Segment: The base was made from 15.9mm thick high density polyethylene (HDPE) (49.5x152.4cm) (Fig. 14a). Ribs are located on the underside of the base, and made from 2.54cm thick HDPE bars. They were designed to mimic the curvature of a GE 1.5T MR scanner couch (General Electric Healthcare, Milwaukee, Wisconsin), and attached to the underside of the base using brass machine screws ($\frac{1}{4}$ -20 x 1"). To prevent the device from translating with respect to the couch, rubber foam strips with adhesive backs were added to the ribs.

Leg Support Assembly: The leg support assembly consists of a leg brace cross pinned to fixed uprights, which are aligned with the knee axis of rotation (Fig. 14a). The uprights house the bearings for the knee rotation shaft, and were constructed of Delrin (acetal copolymer). The uprights were bolted to the base using brass cap screws (5/16-18). The leg brace was made of HDPE and consists of two arms that extend from the uprights, on either side of the shank. It was secured to the uprights using two brass shafts, one on either side of the each upright. The two arms were thermoformed to curve inwards at the distal end, in order to minimize interference with the circular MR bore during maximum knee flexion. The brass shafts, at the base of the leg support, rotate within acetyl-glass ball bearings (P/N A 7Z 5-G1306B, SDP/SI, New Hyde Park, NY). A 45-toothed sprocket (#35 Nylatron GS hubbed roller chain sprocket, SDP/SI) was pinned to the shaft on the medial upright. This drives an acetal roller chain (3/8" pitch, SDP/SI), which connects the leg support assembly to the loading assembly. After the knee joint is

aligned with the knee rotation shaft, the posterior aspect of the subject's ankle is positioned into a concave crossbar, located at the distal end of the two arms. The ankle is then secured using a foam-padded strap with hook-and-loop fasteners.

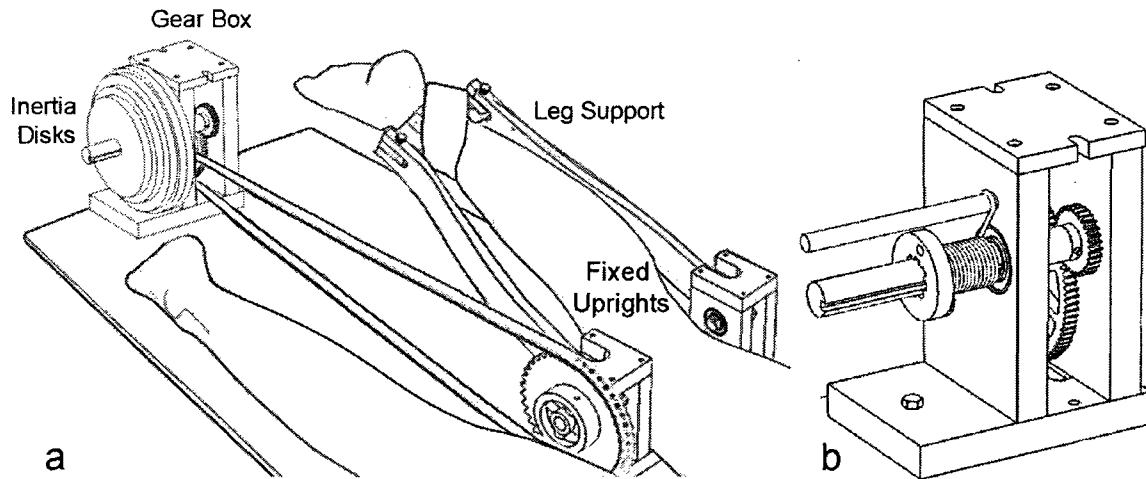


Figure 14: (a) The subject lays prone on the base of the device with their knee joint aligned to an axis of rotation located between two uprights. A large sprocket and chain connect the externally applied loads to the knee. Further amplification of the loads, due to spur gears within the gear box, result in an overall gear ratio of 10:1. As a result, the equivalent inertia at the knee is 100 times greater than the inertia of the disks mounted on the loading shaft. (b) Alternatively, a torsional spring can be mounted on the loading shaft, thereby inducing an elastic load (i.e. shortening contraction).

Loading Assembly: The loading assembly consists of a gear box and a loading shaft. The gear box was constructed of 2.54cm thick HDPE and rigidly attached to the base, just distal of the foot, via brass cap screws (5/16-18) (Fig. 14a). The roller chain drives a 12-toothed sprocket (#35 Nylatron GS hubbed roller chain sprocket, SDP/SI) on an auxiliary brass shaft (1.59cm diameter) within the gear box. Two additional spur gears, located inside the gear box, further amplify the motion of the knee. Specifically, an 80-tooth spur gear (SDP/SI) on the auxiliary shaft meshes with a 30-tooth spur gear (SDP/SI) on a brass loading shaft (2.54cm diameter). This results in an overall gear ratio

of 10:1. Hence, the loading shaft rotates 10 degrees for every one degree of knee rotation. The auxiliary and loading shafts were also mounted on acetyl glass roller bearings fixed to the gear box frame (P/N DP-SI #A 7Z 5-G2010, SDP/SI).

Either circular inertial disks or a torsional spring can be mounted on the loading shaft. As a result of the 10:1 gear ratio, the equivalent inertia or spring stiffness felt by the subject about the knee is 100 (gear ratio squared) times greater than the loads directly generated by the disks or torsional spring. The circular inertial disks (Fig. 14a) were constructed of solid surface material (density, 1574kg/m³; thickness, 1.30cm). Six disks of up to 22.22cm can be mounted on the shaft, allowing for the mass moment of inertia on the shaft to be varied from 0 to 1.92kg-cm² (equivalent inertia varies from 0 to 192kg-cm²). Torsional springs were constructed of stainless steel wire (0.20cm, 0.28cm, and 0.32cm diameter wire with 10-13 turns per spring). The various springs allow the torsional stiffness on the shaft to be varied from 0 to 0.6Nm/rad (equivalent stiffness varies from 0 to 60Nm/rad).

Loading Analysis: In use, subjects are asked to cycle between knee flexion and extension at a rate specified by a metronome. Assuming the motion is harmonic, the knee angle can be expressed as $\theta_k = A \sin \omega t + \bar{\theta}_k$, where t is time in seconds, ω is the angular frequency in rad/sec, $\bar{\theta}_k$ is the average knee angle, A is the amplitude of the motion, and $2A$ is the net knee excursion. The effective internal knee flexion moment, M_k , can then be estimated as:

$$M_k = -\left(I_s + \frac{I_d}{N^2}\right)\omega^2 A \sin \omega t + \frac{k}{N^2} \left(A \sin \omega t + \bar{\theta}_k\right) + m_s g \ell_s^* \cos(\theta_k - \theta_h) \quad [1]$$

where I_s is the moment of inertia of the foot, shank, and leg brace about the knee, m_s is the mass of the foot, shank, and leg brace, ℓ_s^* is the distance from the knee to center of mass of the combined leg and leg brace, I_d is the inertia of the disks, k is the torsional spring stiffness, and θ_h is the hip angle. Of note is that the inertial and elastic components are 180 degrees out of phase with each other. Thus, ignoring the mass of the leg and leg brace, the application of inertial disks on the loading shaft would result in peak knee flexion moments when the knee is extended. In contrast, elastic loading would result in peak knee flexion moments occurring when the knee is fully flexed.

Experimental Testing: The limbs of 10 healthy volunteers were tested (6 females, 4 males; age, 32 ± 11 y; height, 1.75 ± 0.09 m; mass, 70 ± 10 kg). Subjects gave informed consent according to a protocol approved by the University of Wisconsin's Health Sciences Institutional Review Board. Data were collected for each subject's right limb in a motion capture laboratory to evaluate the magnitude and repeatability of motion, loading, and induced muscle activities. Dynamic MR images were later obtained on the each subject's same limb at the University of Wisconsin Hospitals.

Motion Capture: Kinematic, chain tension, and electromyographic (EMG) data were collected while subjects performed cyclic knee flexion-extension while positioned in the device. A semi-circular covering was used to emulate the physical constraints of an MR bore. Kinematic data were collected at 100Hz using an 8-camera passive motion capture system (Motion Analysis; Santa Rosa, CA), and processed using motion capture software (EvaRT v5.0). Knee flexion-extension angle was monitored using markers placed on the device at the axis of rotation of the knee and on the medial and lateral

support arms near the ankle. Two tensile load cells (FT24 Tension Load Cells, Measurement Specialties, Hampton, VA) were attached within the top and bottom portions of the chain to provide a measurement of the chain tension and were used to estimate the effective knee moment.

EMG signals were recorded from the medial hamstrings. Pre-amplified single differential surface electrodes (DE-2.1, DelSys, Inc, Boston, MA), with a fixed 10mm inter-electrode distance, were interfaced with a Bagnoli-16 amplifier/processor unit (CMRR >84dB at 60Hz; input impedance > 100M Ω) and coated with conducting gel prior to application. Electrode locations were prepared by shaving the skin and cleaning with alcohol. Load cell and EMG data were recorded at 2000Hz using a 12 bit A/D converter interfaced with the collection computer.

Subjects were positioned prone in the device with the hip slightly flexed (~14 degrees) so as to elicit a greater stretch of the hamstrings. Each subject performed the cyclic knee flexion-extension at 28 cycles per minute to the beat of a metronome. Following adequate familiarization, subjects completed three two-minute trials for both loading conditions: elastic loading ($k=0.4\text{Nm/rad}$) and inertial loading ($I_d=2.02\text{kg}\cdot\text{cm}^2$). The order of loading conditions was randomized between subjects and all three trials were completed in succession for each loading condition. At least two minutes of rest was given between trials.

The knee angle and load cell data were digitally low-pass filtered at 6Hz (4th order bi-directional Butterworth filter). The knee angle data were then numerically differentiated to estimate the knee angular accelerations. Anthropometric measures were

used to estimate the mass and inertial properties of the lower leg for each subject. Inverse dynamics analysis (with knee angle, angular acceleration, and load cell forces as inputs) was then used to estimate the net internal moment about the knee at each time point during the flexion-extension motion.

Repeatability of the following biomechanical measures were evaluated within and between trials: maximum and minimum knee angle, maximum net internal knee moment, and angle of peak knee moment. These measures were assessed using two-factor (loading condition, trial) repeated measures analysis of variance (ANOVAs). Because dynamic image data are interpolated between the start and end of each flexion-extension cycle to produce the desired number of frames of motion, the cycle-to-cycle variability of the knee angle within each trial must be low. Accordingly, we quantified the standard deviation of the knee angle at 215 (~0.01s sample interval) discrete points throughout the cyclic motion. The average of the 215 standard deviation values are reported in this manuscript.

All EMG signals were full wave rectified and low pass filtered at 6Hz. Signals were normalized to the maximum signal observed for that muscle across any of the six trials. The effect of the loading condition on muscle activity was assessed separately for the flexion and extension phases of the motion. This was done by first finding the mean knee angle for each flexion-extension cycle within each trial. The knee flexion phase was defined as any angle greater than the mean, and the knee extension phase was defined as any angle less than the mean knee angle. Average muscle activity during the flexion and extension phases were calculated for each cycle and averaged across the entire trial. EMG

activity was compared between loading conditions as well as between the flexion and extension phases using paired t-tests.

The magnitude of the induced loading relative to maximum strength was evaluated for each subject. Each subject performed three consecutive isokinetic (30deg/s) knee flexion-extension tasks using an isokinetic dynamometer (Biodex Multi-Joint System 2, Biodex Medical Systems, Inc.). This was done to gauge the magnitude of the induced loading relative to maximum effort.

Dynamic MR Imaging: Cine-PC was used to image the hamstrings and obtain tissue velocities for each subject. Three trials were conducted for each loading condition, using the same loading magnitude as was used in the motion capture laboratory. Images were obtained in a sagittal-oblique plane for six subjects and in a coronal-oblique plane for four subjects. All scans were conducted on a GE 1.5T MR scanner (General Electric Healthcare, Milwaukee, Wisconsin) using a flex wrap coil. The imaging sequence was gated to the onset of knee flexion using a plethysmograph placed under the ankle. Each scan lasted 1min 39s, and resulted in one magnitude image and three velocity images per time frame. Scanning parameters were: voxel size = 1.4x1.4x6mm, VENC = 5cm/s, 256x256 matrix, TR/TE = 21.6/7.1ms, 2 lines of k-space/cycle, 0.45 phase FOV, and 40 reconstructed frames/cycle. Image quality and hamstring tissue velocities were visually compared between subjects and across repeated trials of the same loading condition.

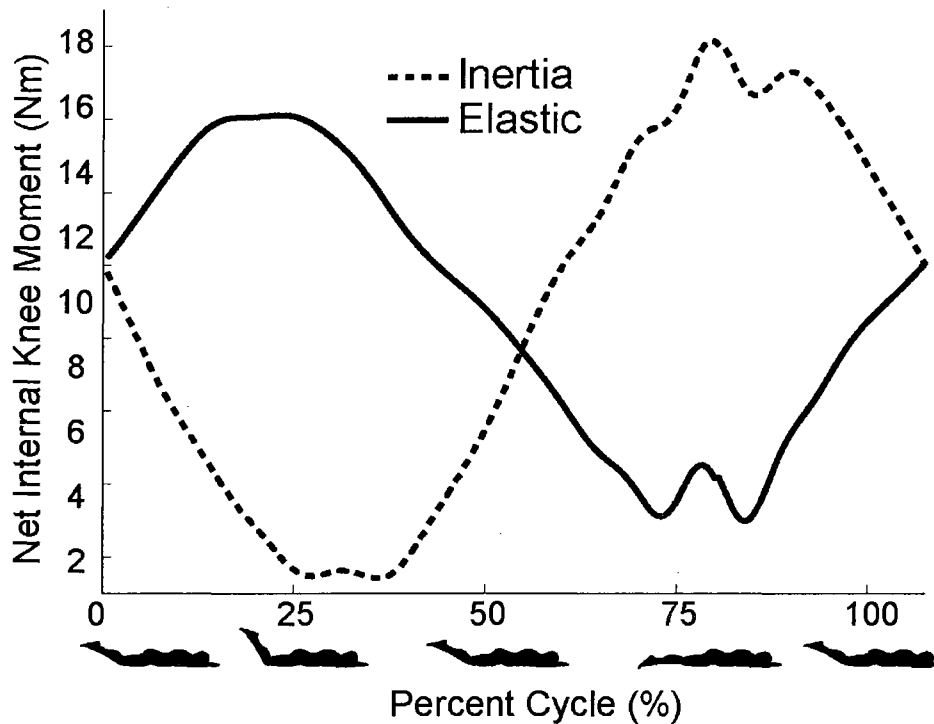


Figure 15: The ensemble averaged net internal knee moments were out of phase between the elastic and inertial loading conditions. The maximum knee flexion moment occurred within two degrees of peak knee flexion during the elastic loading, indicating the muscle is undergoing a shortening contraction. In contrast, the maximum knee flexion moment occurred within one degree of peak knee extension for the inertial loading, indicating that the muscle is undergoing a lengthening contraction.

Results

The MR-compatible limb loading device facilitated repeatable sinusoidal knee flexion-extension motion. Subjects achieved an average of 28.3 ± 4.7 degrees of knee motion, and remained within approximately one degree of their mean knee angle at each point throughout the flexion-extension cycle (a representative trial is given in Table 8). Maximum and minimum knee angle and the angle of peak moment were repeatable to within one degree for each subject (Table 8). These data were also repeatable across trials, with no significant variation for either loading condition ($p < 0.01$).

As predicted by the analytical model (Eq. 1), the knee flexion moment due to elastic and inertial loads were out of phase with each other (Fig. 15). The peak knee flexion moment occurred, on average, within one degree of maximum knee extension for the inertial loading condition and within two degrees of maximum knee flexion for the elastic loading condition. The elastic and inertial loads resulted in effective net knee moments between 10-34% of each subject's maximum isokinetic knee flexion strength ($89.7 \pm 22.3 \text{Nm}$).

Hamstring muscle activity corresponded closely with the net internal knee moment for the elastic load. The inertial loading condition induced two bursts of muscle activity. The first burst occurred as the subjects accelerated the disks during the start of knee flexion. The second burst of muscle activity represented the lengthening muscle contraction, when the subjects decelerated the spinning disks during the second half of knee extension (i.e. before their foot hit the base). These differences between loading conditions were apparent in the averaged flexed and extended knee muscle activities (Fig. 16). Significantly greater muscle activity occurred during knee flexion for the elastic loading condition, and significantly greater activity occurred during the knee extension phase for the inertial loading condition ($p < 0.01$).

Finally, observations made during the dynamic MR imaging experiments confirmed that the device fit safely and securely on the couch and within the bore of the scanner (Fig. 17). Images were obtained with no discernable losses or distortions in the magnetic field or signal-to-noise ratio during scanning. The torsional spring and inertial disks were interchanged on the device without repositioning the subject in the scanner.

The location of the plythesmograph, on the base of the device under the ankle, resulted in clean pulses off which the start of each knee flexion-extension cycle was triggered. Velocity image data revealed systematic differences in tissue velocity along both the length and cross section of the muscle for both loading conditions. However, the inertial loads induced larger velocities in the proximal muscle tissue (10x10mm region of interest), when compared to the elastic loading condition.

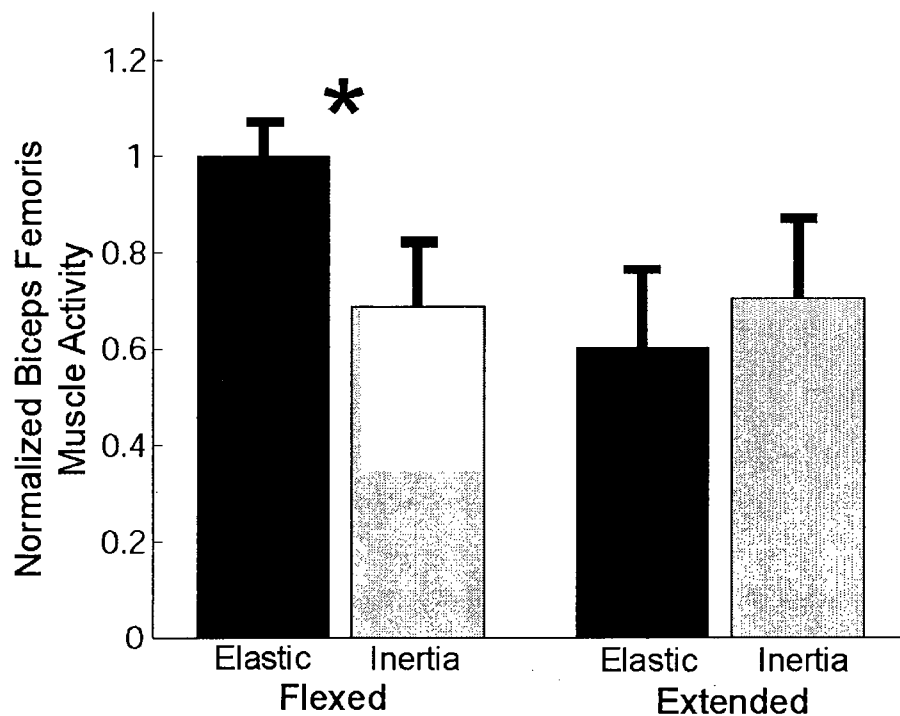


Figure 16: Hamstring EMG measurements indicated that the device can be used to alter the timing of hamstring activity. Mean normalized hamstring activity was significantly greater when the knee was flexed for the elastic loading, but when the knee was extended during the inertial loading condition. The mean muscle activity was significantly greater for the inertial loading condition during the knee extension phase.

Table 8. The mean (SD) measures obtained from one representative trial for each loading condition are presented. Repeatability of joint motion was excellent. Less than one degree of variability was observed for both the maximum and minimum knee angle as well as for the average SD for the entire flexion-extension cycle. The loading conditions induced peak knee moments that were out of phase with each other, such that the peak loading occurred near maximum knee extension for the inertial loading and near peak knee flexion for the elastic loading.

Subject	Loading	Mean SD, Knee Angle (deg)	Maximum knee flexion angle (deg)	Minimum Knee flexion angle (deg)	Angle of Peak Moment (deg)
1	Elastic	0.7	42.6 (0.8)	16.6 (0.6)	39.6 (1.2)
	Inertia	0.6	42.6 (0.8)	17.5 (0.6)	17.8 (1.4)
2	Elastic	0.7	42.2 (0.7)	18.5 (0.9)	41.3 (0.3)
	Inertia	0.9	43.7 (0.8)	18.5 (0.6)	18.7 (0.8)
3	Elastic	1.0	39.6 (0.9)	18.4 (1.0)	38.8 (0.9)
	Inertia	0.7	39.4 (1.1)	18.6 (0.7)	17.9 (0.3)
4	Elastic	0.9	46.5 (0.9)	13.1 (0.8)	43.9 (3.0)
	Inertia	0.8	47.3 (1.0)	15.4 (0.5)	16.7 (0.9)
5	Elastic	1.7	47.6 (2.2)	15.5 (1.2)	43.4 (0.4)
	Inertia	1.4	49.0 (1.8)	17.9 (1.6)	18.0 (1.2)
6	Elastic	0.7	41.3 (1.0)	12.9 (0.5)	40.2 (0.2)
	Inertia	1.0	41.4 (0.9)	14.0 (0.6)	18.3 (2.1)
7	Elastic	1.7	51.5 (0.9)	15.7 (0.5)	48.5 (2.4)
	Inertia	1.6	51.3 (0.9)	13.9 (0.3)	14.3 (0.9)
8	Elastic	2.2	47.4 (1.4)	16.6 (0.5)	46.4 (1.7)
	Inertia	1.7	47.1 (1.3)	17.2 (0.9)	16.7 (1.9)
9	Elastic	2.3	42.6 (1.2)	16.2 (0.7)	43.1 (0.7)
	Inertia	1.4	41.1 (0.9)	17.6 (0.8)	17.7 (1.2)
10	Elastic	1.4	39.7 (0.5)	15.4 (0.7)	37.2 (1.7)
	Inertia	1.3	40.6 (0.9)	13.4 (0.4)	14.3 (0.7)

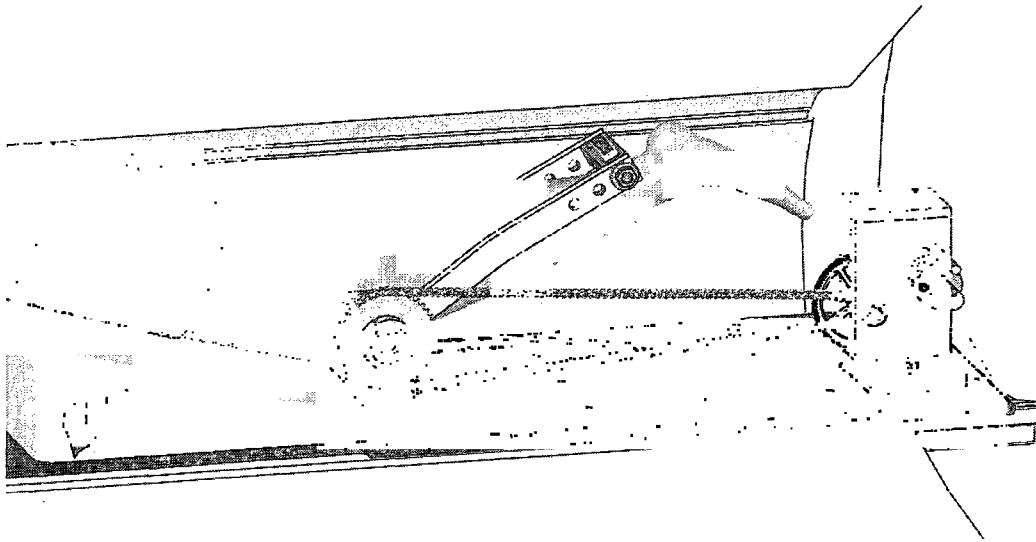


Figure 17: The device fits securely within the bore of a scanner. The gear box is located at the far end of the base, such that the inertial disks and torsional spring can be interchanged without translating the couch between image sequence acquisitions.

Discussion

The results obtained from our testing confirm that the MR compatible device proposed here is capable of inducing smooth, repeatable lower limb motion while Cine-PC MR imaging is performed in the posterior thigh. The use of a torsional spring and inertial disks allows dynamic images to be obtained while muscles undergo either shortening or lengthening contractions. Image data revealed clear differences in tissue velocity between loading conditions in the biceps femoris muscle tissue, near the proximal musculotendon junction. This location is of particular interest, as the majority of hamstring strain injuries occur in this region (Asakawa et al., 2006).

The loads imposed on the limb were less than one-third of maximum isokinetic knee flexion strength. Relatively low loads were used so as not to induce fatigue over the multiple cycles of motion required for Cine-PC imaging (Drace and Pelc, 1994). The device, as designed, is capable of imposing higher loads on the limb than used in this

study. In particular, the utilization of a 10:1 gear ratio greatly increased the loads experienced by the subject, while minimizing the size of the inertial disks and torsional springs needed. Thus, it is feasible to use the proposed device during a real time dynamic imaging sequence (Asakawa et al., 2003) to look at muscle contractions under larger loads. Such a use is important for the assessment of potential injury mechanisms, which tend to occur with muscles near maximal activation and under large external loads (Lieber and Friden, 2002), Finally, having the loading assembly located on the far end of the device allows the type or magnitude of load to be changed between image acquisitions without moving the subject. This feature is important for retaining a constant imaging plane for both loading conditions.

The range of knee motion in the scanner was ~28 degrees. This was limited by both the 60cm bore diameter, as well as the length of the lower limb of the subject. As expected, the subjects with longer limbs had a smaller range of motion. Thus, shorter individuals (i.e. children) or limbs (i.e. the arm) would be able to obtain much larger ranges of motion. In addition, the utilization of this device within a large bore scanner would greatly increase the range of motion that could be obtained. The design of the current device fit securely into a GE 1.5T scanner, but can be easily modified to be used in other scanners (e.g. Siemens or Phillips).

The device was constructed with a variety of different non-ferrous metals, including brass and stainless steel. The metal components were needed to accommodate the loads present in the system. In particular, brass shafts were used for both the knee axis and loading shafts to prevent breakage due to the large shear forces at these locations. We

also manufactured stainless steel torsion springs to generate the elastic load. Finally, the loading assembly was mounted on to two brass rails, so as to allow for the loading assembly to be translated. In this way, it is possible to easily affix and tighten the chain when needed. All of these metal components were located as far from the imaging coil as possible, so as to minimize the potential for image artifacts. One design improvement we are considering is replacing the nylatron roller chain with a Kevlar/urethane flat belt, to increase the stiffness of the connection between the leg support assembly and loading assembly.

The emergence of dynamic imaging capabilities has provided new insights into in-vivo musculotendon mechanics. Previous dynamic MR results have challenged commonly held beliefs regarding fiber shortening (Pappas et al., 2002; Finni et al., 2003), the effects of surgical interventions (Asakawa et al., 2002; Asakawa et al., 2006), and the influence of musculotendon architecture on function (Zhou and Novotny, 2007; Zhong et al., 2008). Other investigators have used ultrasound to ascertain the biomechanical interactions of muscle and tendon during physical tasks such as walking and jumping (Fukunaga et al., 2002). However, limitations of ultrasound make it challenging to implement these procedures more broadly. In particular, a relatively small field of view is available with ultrasound making it difficult to see the entire fiber length of longer muscles such as the hamstrings. Furthermore, ultrasound cannot provide motion measurements outside of the imaging plane. While Cine-PC also cannot track tissue perpendicular of the imaging plane, it does provide the capability of measuring out-of-

plane velocities. This is important for ensuring an imaging plane is chosen in which minimal out-of-plane motion is present.

In conclusion, we believe that using dynamic imaging to investigate different types of loading conditions in skeletal muscle is important to lend additional insight into basic muscle mechanics, injury mechanisms, and surgery planning. For example, it is possible that the difference in tissue motion between lengthening and shortening contractions may impact the ability of the musculotendon to absorb energy during movement, thereby increasing injury risk during lengthening contractions. Furthermore, imaging of individuals with prior muscle injuries (Silder et al., 2008) or surgical procedures (Asakawa et al., 2002; Asakawa et al., 2006) could enable one to quantify how long-term remodeling affects in-vivo musculotendon mechanics.

Chapter 5

The Influence of Prior Hamstring Injury on Lengthening Muscle Tissue Mechanics

Introduction

Acute muscle strain injuries are frequent in sporting activities (Krejci and Koch, 1979; Garrett, 1990). In particular, hamstring strain injuries are extremely common among sprinters and usually involve the proximal musculotendon junction (MTJ) of the biceps femoris long head (BFLH) (Fig. 1) (Schneider-Kolsky et al., 2006; Verrall et al., 2006; Koulouris et al., 2007; Silder et al., 2008). It is well established that muscle strain injuries occur during active lengthening contractions (Garrett, 1990; Lieber et al., 1991; Friden and Lieber, 1998; Kirkendall and Garrett, 2002). Post-injury muscle remodeling processes involve fibrous scar tissue formation at the site of prior injury, which has been shown to persist up to 12 months in animals (Kaariainen et al., 2000). In a recent study on humans, we found evidence that residual scar tissue persists for many months following an athlete's return to sport (Silder et al., 2008). However, it remains unclear whether such remodeling may contribute to the exceptionally high risk for re-injury rate (~30% (Seward et al., 1993)) associated with acute hamstring strain injuries.

Acute muscle strain injuries typically occur along a MTJ (Garrett, 1990; De Smet, 1993; Kaariainen et al., 2000; Rybak and Torriani, 2003). In-situ animal studies have shown that the tear does not actually occur as a result of a separation between muscle and tendon, but rather the body of the muscle fiber is torn, just adjacent to the MTJ (Garrett et

al., 1987). Following injury, contraction of the muscle fibers forms a gap between the ends of the ruptured fibers. The highly vascularized muscle tissue immediately begin the regeneration process of filling this gap (Kaariainen et al., 2000), but by the seventh day, fibrous tissue begins to form and eventually leads to mature acellular scar tissue (Nikolaou et al., 1987; Jarvinen et al., 2005). The scar prevails over the muscle regeneration and the ruptured muscle fibers remain divided into two parts for a very long time, possibly indefinitely. The introduction of scar tissue likely adversely affects forces experienced by nearby muscle tissue (Huijing, 2003).

Prior studies have investigated potential factors associated with hamstring re-injury risk. Biomechanical studies have performed motion analysis of running (Heiderscheit et al., 2005), strength testing (Orchard et al., 1997; Brockett et al., 2001), and musculoskeletal models (Thelen et al., 2005). Previous MR imaging studies have evaluated the location and extent of injury in the acute stage (Gibbs et al., 2004; Koulouris et al., 2007). However, the influence of injury-induced changes in musculotendon morphology on contraction mechanics can only be inferred from static images and these more functional biomechanical measures.

Dynamic MR imaging techniques can be used to track tissue motion and estimate tissue strains *in-vivo*. For example, cine phase contrast (PC) imaging measures the instantaneous tissue velocity using the phase of the acquired signal. PC imaging results in a series of three orthogonal velocity encoded images for each cine frame obtained during a cyclic motion. In the case of skeletal muscle tissue, these data can be integrated to obtain displacements, and subsequently be used to estimate two dimensional (2D) tissue

strains. Dynamic images obtained during contractions of healthy muscle have highlighted the heterogeneous nature of tissue strain along the length of the muscle, and strong dependence on both tissue properties and morphology (Asakawa et al., 2003; Blemker et al., 2005; Butterfield and Herzog, 2005; Zhou and Novotny, 2007). Thus, it is likely that post-injury remodeling would affect local contraction mechanics, and potentially contribute to the risk of muscle strain re-injury.

For this study, cine-PC imaging was used to measure three-dimensional tissue velocities in the proximal biceps femoris during knee flexion-extension. Analysis of the images was used to quantify the displacement and strain distributions in the muscle tissue, and to test our hypothesis that increased strain exists along the proximal musculotendon boundary. Two types of muscle contractions were compared: an active lengthening condition and a relaxing and lengthening condition. To further understand the influence of scar tissue on local muscle tissue mechanics, both healthy control athletes and those with a prior hamstring injury were tested.

Methods

The right limbs of 11 healthy subjects (6 females, 5 males; age 31 ± 11 y; height 1.77 ± 0.09 m; mass 70 ± 9 kg) and the previously injured limbs of four subjects (4 males, age 24 ± 8 ; height 1.88 ± 0.07 ; mass 84 ± 4 kg) were tested. The location and method of injury were obtained via subject questioning and clinical reports. Additionally, MR images at the time of injury were available from two of the four subjects and were used to confirm injury descriptors given by the subjects and clinical reports. All subjects gave informed consent according to a protocol approved by the University of Wisconsin's

Health Sciences Institutional Review Board. All scans were conducted on a GE 1.5T MR scanner (General Electric Healthcare, Milwaukee, Wisconsin).

Before dynamic image acquisitions, static iterative decomposition of water and fat with echo asymmetry and least-squares estimation (IDEAL) (Reeder et al., 2005) images were acquired of both limbs using a phased array torso coil, with the subject in a relaxed prone position. Scan parameters were TR/TE_{eff}, 12.7/4.4; 15° flip angle; matrix, 512x512; 1.5 NEX; 0.7mm coronal slice thickness, no gap. Bilateral differences in tendon volume were quantified for the healthy control subjects as well as the previously injured subjects with unilateral injuries (Silder et al., 2008). Inter-subject variability in muscle and tendon morphology was qualitatively evaluated.

Each subject was then repositioned to lay prone on a MR-compatible device (Fig. 14) (Silder et al., 2009). The hip was flexed to ~15 degrees to allow for a range of knee motion with greater hamstring stretch. The knee joint was aligned to an axis of rotation and the ankle was secured to two leg braces that extended from the knee rotation shaft. The range of knee motion was ~30 degrees. The device was designed to guide the limb through cyclic knee flexion-extension while imposing either inertial (Fig. 14a) or elastic (Fig. 14b) load on the hamstrings. In a prior study, we showed that the device induces repeatable motion and generates muscle activity during knee extension such that the inertial loading induces active lengthening contractions, and the elastic loading induces relaxing and lengthening contractions (Silder et al., 2009). Specifically, for the inertial loading, peak hamstring activity occurred at full knee extension, and for the elastic loading, peak hamstring activity occurred at full knee flexion.

Cine-PC imaging was used to measure tissue velocities within an imaging plane that bisected the long axis of the biceps femoris. An oblique-sagittal plane was used for six healthy subjects and an oblique- coronal plane for the remaining five healthy and four previously injured subjects. All images were collected using a flex wrap coil secured around the posterior thigh. Three trials were conducted for each loading condition at a rate of 28 cycles/min using peak loads of ~20% of each subject's isokinetic knee flexion strength (30deg/sec) (Silder et al., 2009). The imaging sequence was gated to the onset of knee flexion using a plethysmograph placed under the ankle. Each scan lasted 1min 39s, and resulted in one magnitude image and three velocity images per time frame. Scanning parameters were: voxel size = 1.4x1.4x6mm, VENC = 5cm/s, 256x256 matrix, TR/TE = 21.6/7.1ms, 2 lines of k-space/cycle, 0.45 phase FOV, and 40 reconstructed frames/cycle.

Reconstruction of the PC images was performed online, and subsequent displacement and strain analyses were performed offline using MATLAB (The Mathworks Inc., Natick, MA, USA). Dynamic images were analyzed using a mesh based tracking approach (Zhu and Pelc, 1999). For each trial, we first manually identified a region of interest over the visible portion of the BFLH, using a frame when the knee was fully flexed. An initial mesh was generated within this region using triangular linear strain elements (edge lengths of ~5mm) (Fig. 18a). This initial mesh was considered the reference configuration for all subsequent analyses. At each frame, element shape functions were used to express the pixel velocities within each element as a linear function of nodal velocities. Linear least-squares was then used to solve for the nodal velocities that generated pixel velocity estimates that most closely agreed with measured

values. Nodal displacement trajectories were subsequently obtained by using forward-backward integration (Pelc et al., 1995), followed by closed-loop Fourier integration (Zhu et al., 1996) of the nodal velocities. The resulting nodal trajectories, along with the linear finite-element shape functions, uniquely specified the mesh configuration and deformation at each frame in the motion (Zhu and Pelc, 1999).

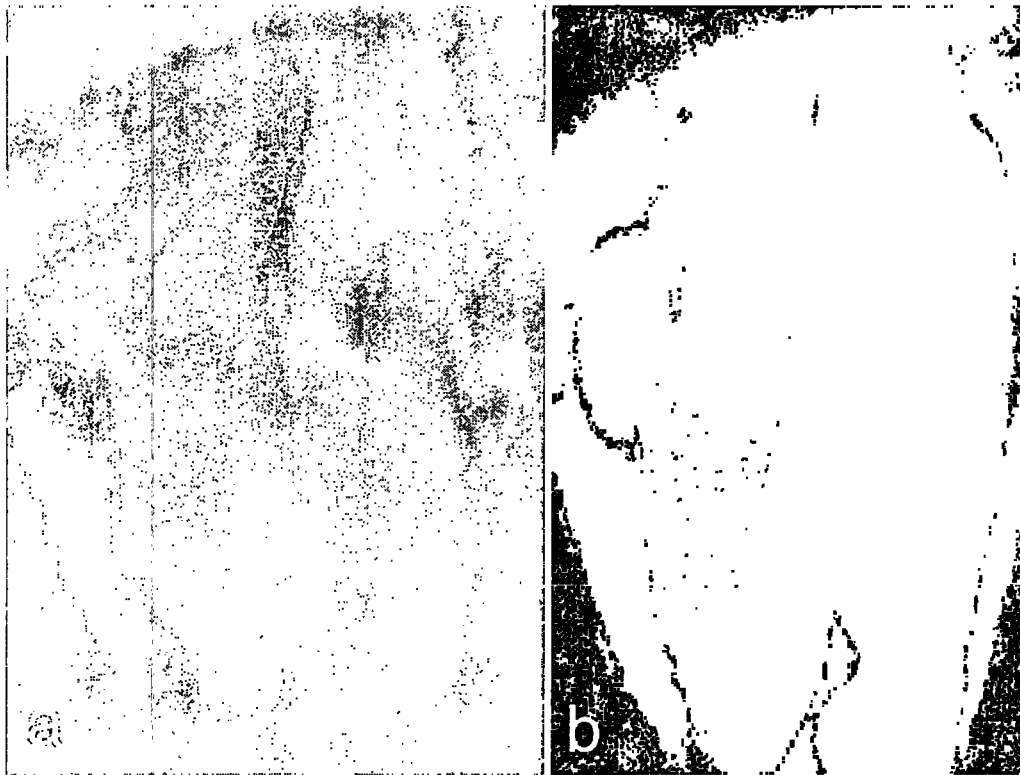


Figure 18: (a) A mesh based tracking approach was used to compute tissue motion within the long head of the biceps femoris. (b) Four distinct spatial regions were defined for each subject, based on the distance the tissue was from the proximal musculotendon junction. This allowed for quantitative analysis of displacement and strain measures relative to the musculotendon junction.

To analyze the 2D strain fields, the Lagrangian finite strain tensor \mathbf{E} was calculated using the deformation gradient tensor. After diagonalization of \mathbf{E} , the directions of the first and second principal strains and the corresponding eigenvalues, E_1 and E_2 , were found, where the negative and positive eigenvalues were assigned to the first and second principal strains, respectively. The directions of the first and second principal strains were expressed as the angle between the strain vector and the inferior longitudinal axis of the imaging plane.

In order to quantify the distribution of muscle displacements and strains relative to the proximal MTJ, a series of four regions were defined within the muscle tissue. Using the magnitude image from the frame corresponding to maximum knee flexion (i.e. the reference configuration), a line was manually drawn along the length of the visible tendon. Areas of tissue were defined between 0-1cm, 1-2cm, 2-3cm, and 3-4cm from the line representing the tendon (Fig 18b).

Data were quantified using both whole muscle and regional averages. Statistical comparisons were made between loading conditions, groups, and muscle regions for maximum tissue displacement and maximum E_1 magnitude and corresponding direction using repeated measures ANOVAs.

Results

Morphological features of the proximal hamstring tendons and biceps femoris muscle tissue varied among the subjects. Unpublished observations suggest differences exist in the length and thickness of the proximal tendon and aponeurosis as well as the length and maximum cross sectional area of the BFLH muscle tissue. Static images

confirmed that the all previously injured subjects sustained at least one injury to the proximal BFLH (Table 9). The proximal tendon/aponeurosis volumes for the two previously injured subjects with unilateral injuries were 49% and 139% larger than the uninjured limb, compared to an average difference of 12% between limbs in the healthy subjects. The remaining previously injured subjects exhibited substantial scarring adjacent to the proximal tendon, when assessed using the static MR images (Fig. 19).

Table 9: Descriptors of injury characteristics from the four subjects with prior hamstring strain injuries. Only subjects with at least one injury to the proximal biceps femoris were included in this study.

Subject	Number of Injuries	Method of Injury	Muscle(s) Injured
1	1	sprinting	1 st and 2 nd injuries: proximal biceps femoris
2	2	sprinting	1 st injury: proximal biceps femoris and mid-semitendinosus 2 nd injury: proximal biceps femoris
3	1	high jump approach	proximal biceps femoris
4	2	hurdles	1 st injury: mid-semitendinosus 2 nd injury: proximal biceps femoris

Displacements and strain magnitudes were similar between the two imaging planes (i.e. oblique-coronal or oblique-sagittal). Repeat acquisitions of the same loading condition resulted in displacement and strain estimates with similar values and appearance, indicating good repeatability of the motion and data analysis techniques (Fig. 20).

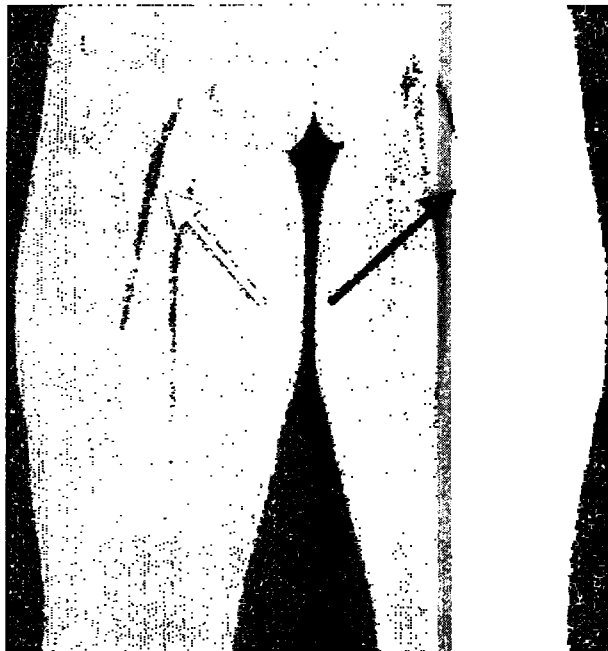


Figure 19: A substantial amount of scar tissue was visible adjacent to the side of prior injury (white arrow) for all four previously injured subjects. One of the two subjects with bilateral injuries is shown.

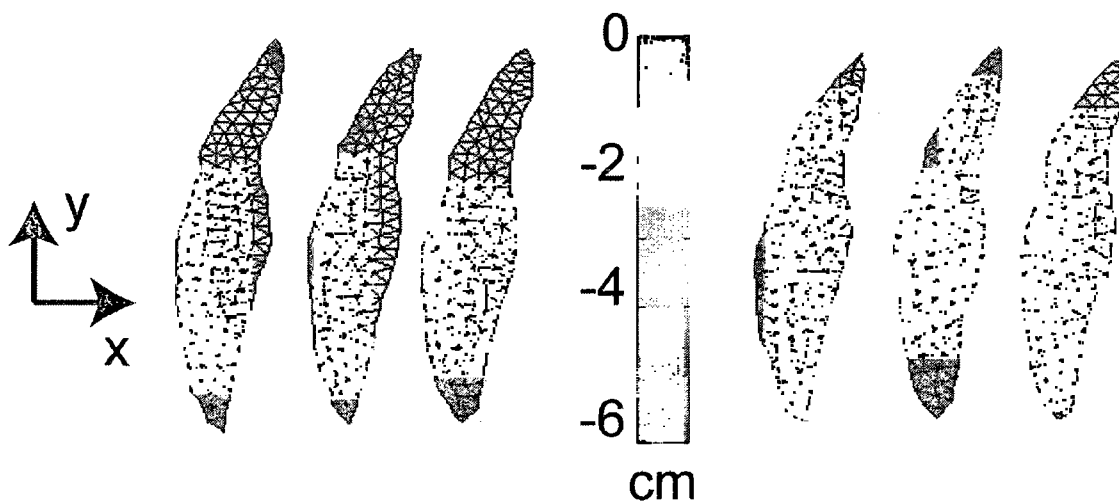


Figure 20: Repeatability of vertical tissue displacements computed for repeat (a) elastic and (b) inertial loading trials was very good, with differences between loading conditions readily apparent. In particular, the (b) active lengthening contractions (inertial load) induced more isometric tissue motion, compared to the (a) relaxing and lengthening contraction (elastic load).

Although the magnitude of tissue motion varied between subjects (Fig. 21), the general pattern along the length and width of the muscle was similar between subjects for each loading condition. Statistical analysis of tissue displacements showed that, for both loading conditions, the smallest tissue motion was observed along the proximal MTJ ($p < 0.01$) (Fig. 20). Differences between loading conditions were apparent, with relatively greater motion measured along the proximal MTJ for the inertial loading ($p = 0.02$), when compared to the elastic loading condition. This resulted in a more uniform vertical displacement field across the muscle for the inertial condition (Fig. 20). When only considering the healthy control subjects, whole muscle displacements were significantly greater for the inertial loading condition ($p = 0.03$). However, with the inclusion of the four previously injured subjects, this difference was no longer significant ($p = 0.12$). The directions of the first principal strains were generally aligned with fiber direction, as ascertained from the static images (Fig 22). No significant differences were observed for the directions of the first principal strains between groups. However, first principal strain directions were clearly different between imaging planes (i.e. oblique-sagittal or oblique-coronal) as well as between the right limbs of the healthy control subjects imaged in an oblique-coronal plane and the previously injured subjects with left limb injuries.

Average muscle tissue strains across the entire muscle were on the order of ~10% (Fig. 23). For both groups, peak first principal strain values were significantly greater for the elastic loading ($p=0.03$). Regional comparisons revealed that muscle tissue adjacent to the proximal MTJ experienced greater tensile strains ($p<0.01$) than tissue further away (Fig. 23). These regional variations were exaggerated for the previously injured subjects. Specifically, tissue strains were significantly greater for the previously injured subjects across all regions ($p=0.03$) (Fig. 24).

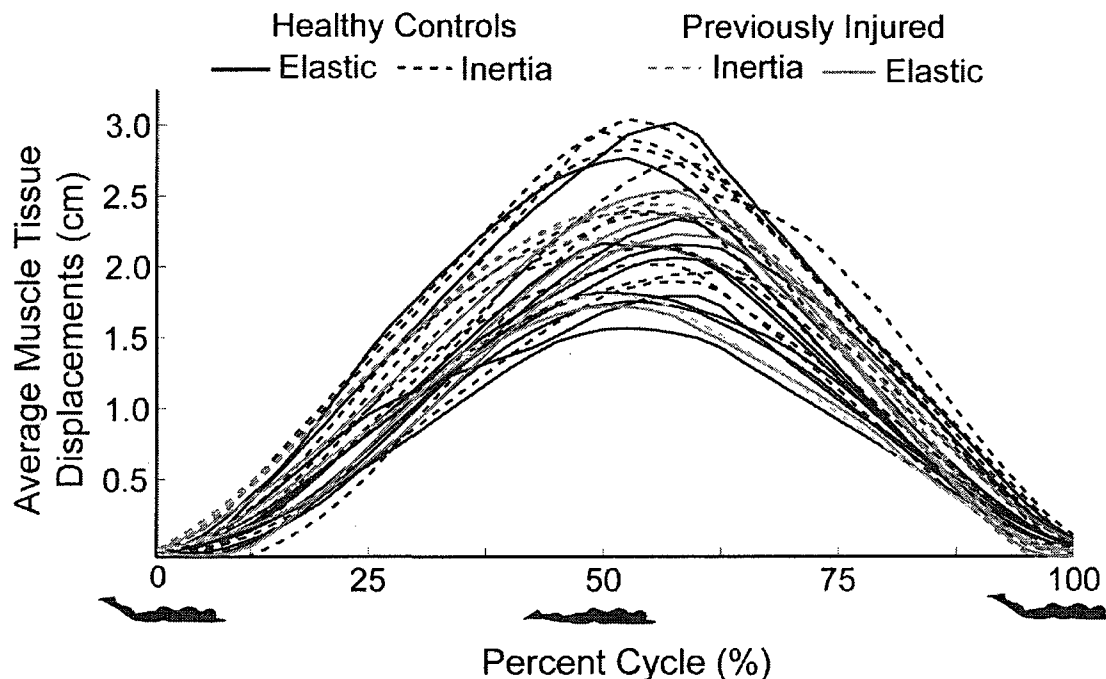


Figure 21: Inter-subject variability was evident in line traces representing vertical muscle tissue displacement. These differences were most likely largely a result of subject height, which translated into range of knee motion within the scanner.

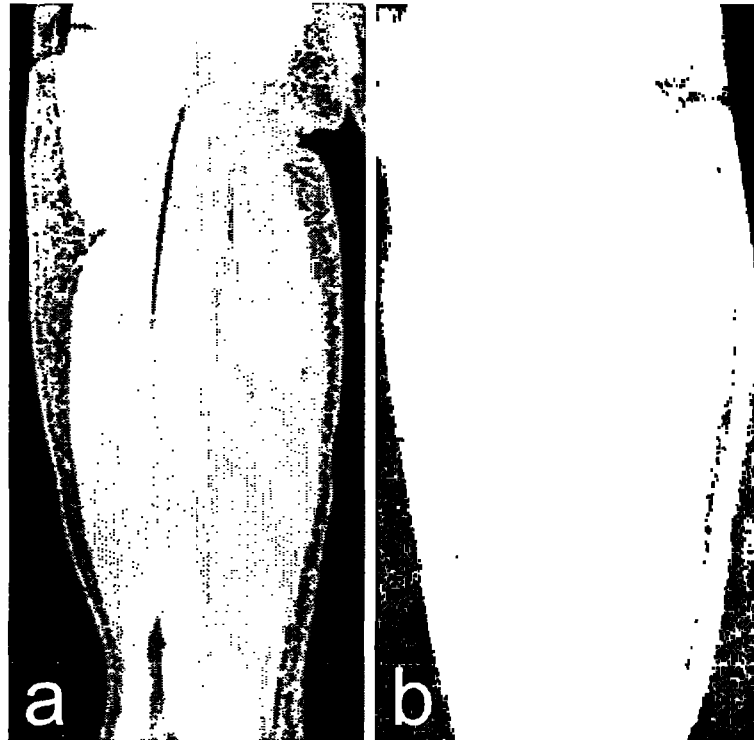


Figure 22: (a) High resolution static images were obtained for all subjects and used to visualize muscle fiber directions. (b) The directions of the first principal strains were generally aligned with fiber direction, suggesting primarily along fiber stretch was occurring.

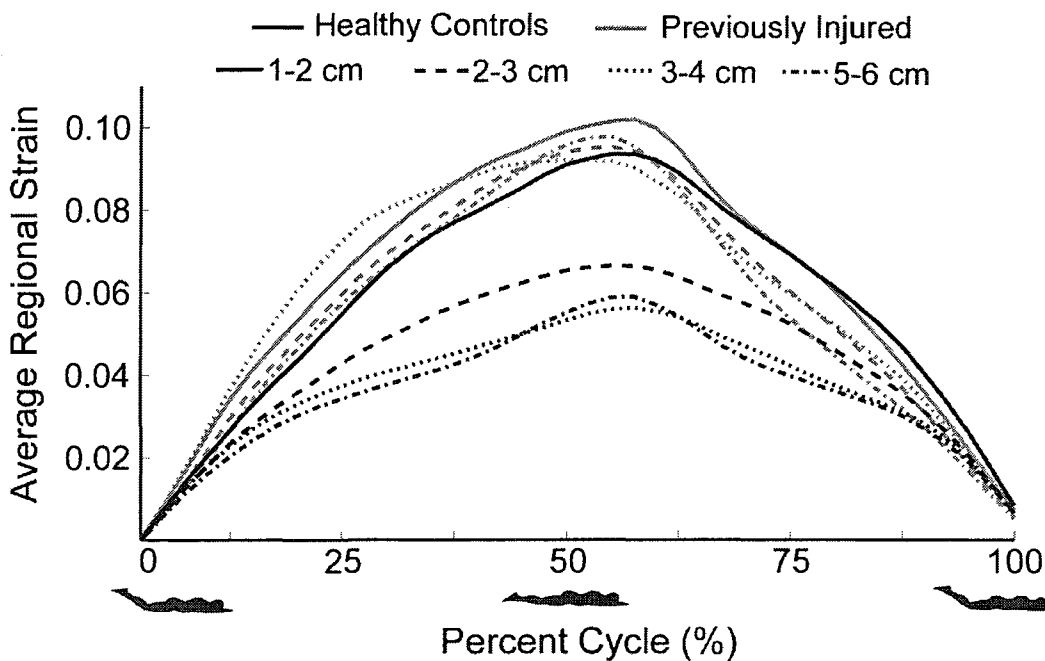


Figure 23: Average first principal strains (E_1) within each region were significantly greater for the elastic loading condition. For both loading conditions, the largest tensile strains occurred immediately adjacent to the musculotendon junction.

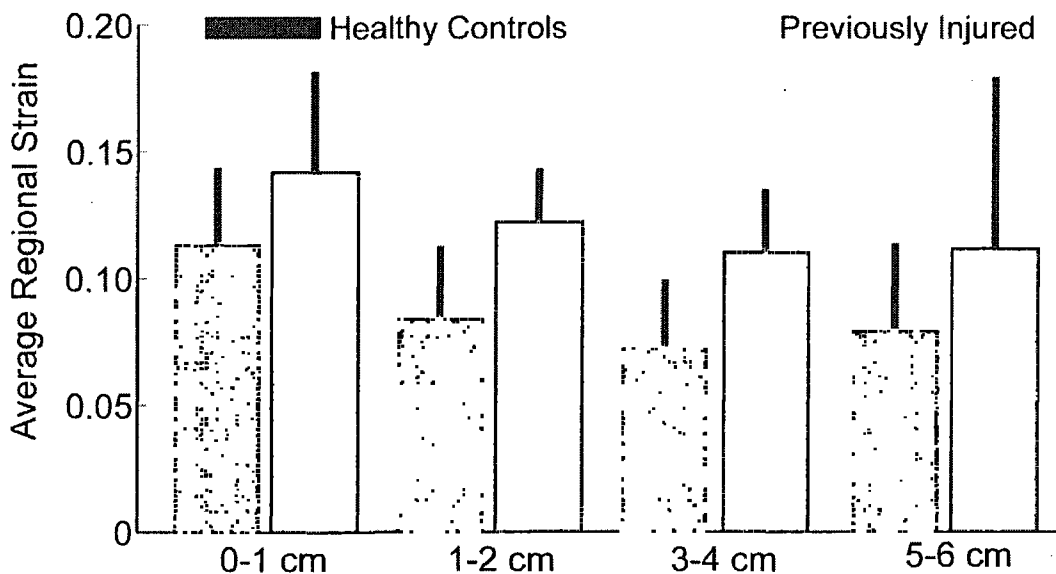


Figure 24: First principal tissue strains (E_1) were significantly greater for the previously injured subjects in all regions compared. These results suggest that remodeling processes from the prior injury may affect surrounding muscle tissue mechanics.

Discussion

The overall goal of this study was to investigate the influence of scar tissue on *in-vivo* mechanical strains in the biceps femoris long head. Lagrangian strains were estimated during muscle contractions during which the muscle was both active and lengthening (inertial load) or relaxing and lengthening (elastic load). We hypothesized that the presence of scar tissue in subjects with a prior hamstring strain injury would produce greater localized strains along the proximal MTJ, when compared to healthy uninjured subjects. Indeed, for both subjects groups, the largest strains were observed along the proximal MTJ and, subjects with a prior injury exhibited significantly greater strains in this region. These results are of particular interest clinically, as they give insight into how scar tissue can alter contraction mechanics along the MTJ and potentially contribute to re-injury risk.

In un-injured muscle, as fibers approach the MTJ, extensive folding of the sarcolemma increases the surface area available for force transmission to the tendon (Kaariainen et al., 2000). This helps make the MTJ very compliant in tension (Purslow, 2002). However, during injury the sarcolemma is usually damaged, which results in fibrous scar formation, and hence, disruption of the functional capacity of the muscle-tendon interaction to transmit forces (Best and Hunter, 2000). In the current study, we measured significantly greater strains in subjects with substantial scarring along the previously injured MTJ. The presence of scar tissue creates much stiffer conditions, when compared to an un-injured MTJ (Purslow, 2002). It is likely that these remodeling

processes along the MTJ alter the muscle-tendon interaction, necessitating greater stretch in fibers adjacent to the previously injured MTJ.

The displacement and strain fields estimated in this study showed substantial variation throughout the length and width of the muscle, which is consistent with observations made in prior dynamic imaging studies (Asakawa et al., 2002; Pappas et al., 2002; Blemker et al., 2005). To the best of our knowledge, this is the first study to use dynamic MRI to systematically compare contraction mechanics under altered loading conditions. Clear differences were evident, with larger proximal tissue displacements when the muscle was active and lengthening (inertial load), compared to when it was relaxing and lengthening (elastic load). This difference is likely attributable to increased proximal tendon stretch during the active lengthening contractions, which allows the muscle fibers to remain relatively isometric (Fukunaga et al., 2001; Reeves and Narici, 2003). These results were confirmed by our findings of greater overall muscle motion during the active lengthening contractions, compared to the relaxing and lengthening contractions. Furthermore, the first principal strains were significantly greater for the elastic loading condition, indicating a more isometric muscle during the active lengthening contraction. Since muscle tissue remains mostly isometric during the lengthening phase of stretch-shortening cycles, the strain in the muscle tissue is thought to be largely dependent on the properties of the tendons (Lieber et al., 1991; Thelen et al., 2005; Fukashiro et al., 2006). For example, a tendon with high compliance infers that the stretch of the muscle-tendon complex would be taken up mostly by the tendon.

Conversely, an increase in the mechanical stiffness of the tendon-aponeurosis complex, such as following injury, may cause increased strain in nearby muscle tissue.

For both loading conditions and subject groups, the directions of the first principal strains were consistently aligned with the fiber direction (as could be ascertained from the static images), implying a positive first principal strain represents along fiber stretch. Though similar in direction, variability was observed in the magnitude of displacements and strains among some subjects (Fig. 21). Some of these differences were likely a result of variability between subjects with respect to range of motion within the scanner, tendon/aponeurosis thickness, and muscle size. Individual differences in muscle and connective tissue structure as related to the heterogeneous behavior of muscle tissue motion should be explored further, however is beyond the scope of this study.

Collagenous tissue, such as tendon/scar, is void of signal in MR imaging and appears as regions of high noise in cine-PC velocity data. As a result, tracking the motion of pixels immediately adjacent to this noise presents a considerable challenge. One prior study used regions of interest (ROI) within very close proximity to the tendon/aponeurosis and assumed the ROIs were accurately representative of the neighboring tendon/aponeurosis motion (Finni et al., 2003). Since noise in the velocity data degrades reconstructed displacement trajectories, the tracking of ROIs will result in position errors that amplify with time. Hence, the path of a ROI along a muscle-tissue boundary may leave the muscle boundary or include pixels from the neighboring tendon, thereby inducing large artificial motion. In this study, we use a global model using velocity samples from the entire BFLH muscle area at all time frames, which can be more

reproducible and more efficient in estimating the whole-body displacement and strain fields (Zhu and Pelc, 1999).

There were several potential limitations to this study. First, the reliability of displacement data from cine-PC imaging depends on the subject's ability to perform repeatable flexion-extension motion with minimal fatigue. Prior to imaging experiments, we established that both the induced loads and muscle activities were highly repeatable when tested outside of the scanner, with less than one degree variation in peak knee motion over 50+ cycles (Silder et al., 2009). Fatigue effects were addressed by using relatively low loads, requiring ~ 20% of the subject's maximum knee flexion strength. Visual analysis and statistical comparisons of repeat image collections revealed no significant differences between trials, (Fig. 20), suggesting that fatigue effects were small. Second, our analysis of tissue motion inherently assumes that the predominate muscle tissue motion occurs within an imaging plane. The average absolute value of out-of-plane displacement for was 24% of the velocity in the S-I direction, which is similar to the values reported for out-of-plane velocities in previous studies (Sheehan et al., 1998; Pappas et al., 2002; Zhou and Novotny, 2007).

Third, caution must be taken when interpreting the strain magnitudes. We computed strains relative to the muscle's configuration at maximum knee flexion, which does not reflect the relaxed muscle configuration and is not consistent across loading conditions. In particular at full knee flexion, the muscle was active for the elastic loading condition, and relatively relaxed for the inertial loading condition (Silder et al., 2009).

This would, in turn, necessitate greater muscle lengthening for the elastic loading condition when the knee is relaxing and lengthening.

Finally, we were not able to define a single cross-section that encompassed the entire length of the BFLH musculotendon, which extends from the ischial tuberosity down to the fibular head and lateral tibial condyle. Instead, we constructed the imaging plane to clearly bias the proximal BFLH tendon and aponeurosis while extending down the length of the muscle as far as possible. As a result, the regional strains and displacement maps do not reflect the behavior of the entire cross-sectional area of the tendon or muscle, but a portion. The development of methods to acquire 3D volumetric data in an acceptable scan time would circumvent this problem, and provide means of evaluating 3D strains through the muscle volume (Wentland, Korosec, Grist, 2006). Recently, several investigators have developed finite-element models of skeletal muscle that account for 3D geometries, fiber descriptions, and are able to characterize non-uniform shortening within muscles (Blemker and Delp, 2005; Fernandez et al., 2005; Yucesoy and Huijing, 2007). The study of 3D strain distributions in muscle is important for understanding its function under both healthy and pathological conditions, and can lend additional insights into activation strategies and injury mechanisms.

Simulations of running have shown that the hamstrings undergo a stretch-shortening contraction when decelerating the limb during the latter half of swing (Thelen et al., 2005), which is likely when the hamstrings are susceptible to injury (Heiderscheit et al., 2005). The current study showed that increased mechanical strains arise near the proximal biceps femoris MTJ during relatively low-load lengthening contractions, and

that subjects with prior injury presented with significantly greater strains in this region, when compared to their healthy counterparts. Thus, the results suggests that residual scar tissue at the site of a prior musculotendon injury may adversely affect local tissue mechanics in a way that could contribute to risk for re-injury during movement tasks (e.g. running) that involve active lengthening contractions.

CONCLUSIONS

Throughout this dissertation, a potpourri of measurement and analysis techniques were utilized to investigate the effects of a prior hamstring injury on musculotendon morphology, biomechanical function, and in-vivo muscle tissue mechanics. Although we accomplished a great deal, much remains to be learned regarding the mechanism of hamstring injury, factors associated with injury and re-injury risk, optimal rehabilitation techniques and return to sport criteria, and how morphological changes associated with injury may influence re-injury risk. It is unflappable that the ultimate goal is to minimize re-injury rate, while at the same time allowing athletes to return to sport as quickly and effectively as possible. These next few pages will encapsulate my dissertation by briefly capitulating future directions for research, which will help to juxtapose the sometimes disparate areas of radiology, biomechanics, and clinical care.

Static MR imaging is widely used clinically to assess copious musculoskeletal injuries, most commonly involving the knee and shoulder. However, most athletes do not seek medical attention for muscle strain injuries and even fewer obtain an MRI at the time of injury. This is mostly due to the cost and availability of MR scanners, which makes it ersatz to other diagnosis approaches for these injuries. Therefore, research utilizing static MRI should focus on correlating findings to clinical applications such as treatment and optimizing return to sport criteria. Chapter 1 utilized MR imaging to investigate the long term changes in musculotendon morphology following a hamstring strain injury. We found a significant increase in the size of the tendon/aponeurosis on the side of prior injury. At this time, MR imaging is constrained in its ability to distinguish

tendon from scar. Thus, we attributed an increase in tendon volume to scar tissue formation, and determined significance via comparisons with healthy un-injured athletes.

The same subjects that obtained static MR images (Chapter 1) also participated in an extensive series of biomechanical tests utilizing motion analysis and strength testing. Although significant bilateral differences were measured with respect to muscle and tendon volumes between the injured and uninjured limbs of the previously injured subjects, these differences were not consistently represented in the joint level measures. Motion capture techniques assume that a finite number of surface markers can accurately represent bony landmarks of the body. These bony landmarks are then used to calculate joint angles and estimate musculotendon lengths. Throughout this process, errors can occur in marker placement with respect to anatomical structures and skin motion artifact. Finally, subjects in this study ran on a high speed treadmill. Subtle differences between treadmill sprinting and over-ground running are not currently known, and it is likely that some of the participating subjects altered their running techniques during the testing procedure. Advances in motion capture modeling techniques will pacify many of these quagmires, making these methods more pragmatic.

As part of the biomechanical testing protocol, isokinetic knee flexion-extension strength testing was conducted for each subject at 60 deg/sec with the hip flexed at 90deg (Chapter 3). Strength testing can be extremely insightful, but may not reflect the particular muscle of interest. For example, during manual muscle testing one can manipulate factors such as internal/external rotation and hip angle, which can better isolate individual muscles. Isokinetic strength testing allows the athlete to compensate,

thereby maintaining overall knee flexion strength. Ideally, isokinetic strength testing protocols would include multiple hip angles, multiple speeds, as well as concentric and eccentric portions. Unfortunately, this type of protocol would take a dreadfully long time and produce significant fatigue because tests are done at maximum strength.

We began using dynamic MR imaging, in part, because it permits exploration of in-vivo muscle tissue mechanics. In Chapter 4, we designed and built a MR compatible device to load the limb during cyclic knee flexion-extension tasks. In order to obtain adequate spatial resolution, current dynamic MR imaging requires the use of multiple repeatable cycles. As a result, low loads must be used to minimize fatigue effects. Furthermore, the 60cm bore of the GE 1.5T scanner used in this dissertation limits the range of joint motion available within the scanner. Improved real time imaging techniques, higher strength magnets, and large bore scanners would be splendid improvements to our methods.

Finally, being an engineering-based dissertation, the primary focus has been on measuring and modeling biomechanical function. However, numerous prior studies have acknowledged the importance nutrition on muscle recovery and function. Of particular interest is the correlation between nutrition and muscle tissue regeneration. Encouraging appropriate eating habits during sports training and rehabilitation is an area of particular importance to me (Appendix B).

In conclusion, I really enjoyed working on the studies presented here as well as being the impetus for other projects that were not included in this dissertation including: the old and young walkers, subjects with acute hamstring injuries (AHIs), and the

triathlon (TRY) performance study, and encouraging the unprecedented development of the ambulatory mass model of young walking with roller feet (AMY) and Mr. and Mrs. Little Man (Fig 25).

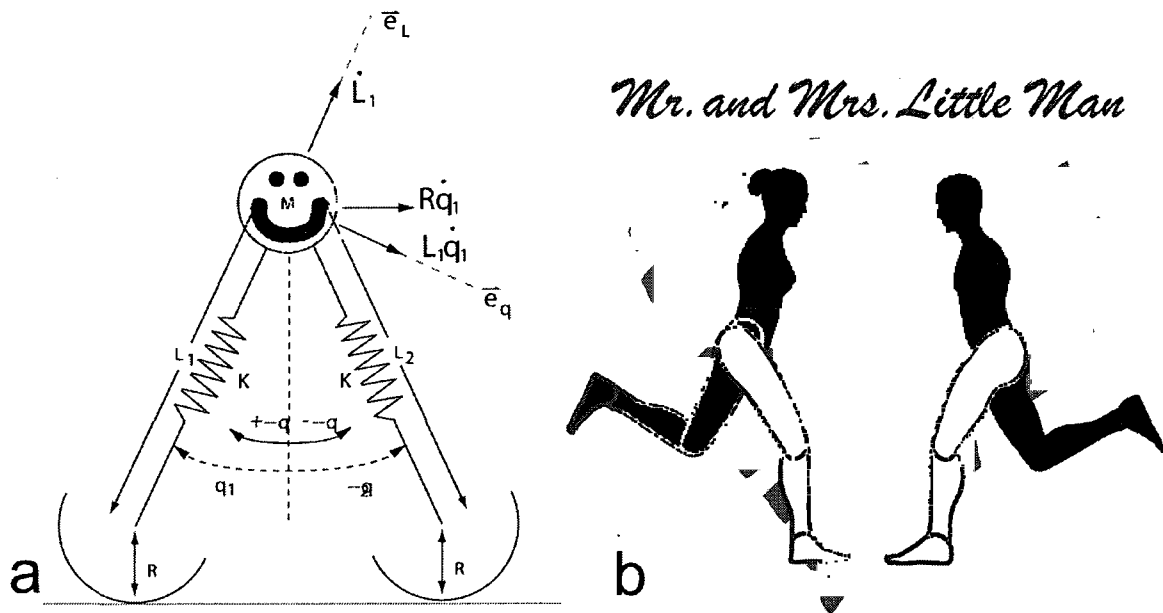


Figure 25: (a) The ambulatory mass model of young walking with roller feet (AMY) was introduced by Whittington and Thelen (Whittington and Thelen, 2009) and allowed for accurate representation of ground reaction forces by a point mass model of walking. (b) Little Man recently met Mrs. Little Man when a select group of biomechanics researchers were concerned about gender equality.

REFERENCES

- Agre, J.C., 1985. Hamstring injuries. Proposed aetiological factors, prevention, and treatment. *Sports Med* 2(1): 21-33.
- Arnason, A., Sigurdsson, S.B., Gudmundsson, A., Holme, I., Engebretsen, L.Bahr, R., 2004. Risk factors for injuries in football. *Am J Sports Med* 32(1 Suppl): 5S-16S.
- Asakawa, D.S., Blemker, S.S., Gold, G.E.Delp, S.L., 2002. In vivo motion of the rectus femoris muscle after tendon transfer surgery. *J Biomech* 35(8): 1029-1037.
- Asakawa, D.S., Blemker, S.S., Gold, G.E.Delp, S.L., 2006. Dynamic magnetic resonance imaging of muscle function after surgery. *Skeletal Radiol* 35(12): 885-886.
- Asakawa, D.S., Nayak, K.S., Blemker, S.S., Delp, S.L., Pauly, J.M., Nishimura, D.G.Gold, G.E., 2003. Real-time imaging of skeletal muscle velocity. *J Magn Reson Imaging* 18(6): 734-739.
- Asakawa, D.S., Pappas, G.P., Blemker, S.S., Drace, J.E.Delp, S.L., 2003. Cine phase-contrast magnetic resonance imaging as a tool for quantification of skeletal muscle motion. *Seminars in Musculoskeletal Radiology* 7(4): 287-295.
- Asakawa, D.S., Pappas, G.P., Blemker, S.S., Drace, J.E.Delp, S.L., 2003. Cine phase-contrast magnetic resonance imaging as a tool for quantification of skeletal muscle motion. *Semin Musculoskelet Radiol* 7(4): 287-295.
- Askling, C.M., Tengvar, M., Saartok, T.Thorstensson, A., 2007. Acute first-time hamstring strains during slow-speed stretching: clinical, magnetic resonance imaging, and recovery characteristics. *Am J Sports Med* 35(10): 1716-1724.
- Basmajian, J.V., De Luca, C. J., 1985. *Muscles Alive: Their Functions Revealed by Electromyography*. Williams & Wilkins, Baltimore.
- Best, T.M.Hunter, K.D., 2000. Muscle injury and repair. *Phys Med Rehabil Clin N Am* 11(2): 251-266.
- Best, T.M., Shehadeh, S.E., Levenson, G., Michel, J.T., Corr, D.T.Aeschlimann, D., 2001. Analysis of changes in mRNA levels of myoblast- and fibroblast-derived gene products in healing skeletal muscle using quantitative reverse transcription-polymerase chain reaction. *Journal of Orthopaedic Research* 19(4): 565-572.
- Blemker, S.S.Delp, S.L., 2005. Three-dimensional representation of complex muscle architectures and geometries. *Ann Biomed Eng* 33(5): 661-673.
- Blemker, S.S., Pinsky, P.M.Delp, S.L., 2005. A 3D model of muscle reveals the causes of nonuniform strains in the biceps brachii. *J Biomech* 38(4): 657-665.
- Bordalo-Rodrigues, M.Rosenberg, Z.S., 2005. MR imaging of the proximal rectus femoris musculotendinous unit. *Magn Reson Imaging Clin N Am* 13(4): 717-725.
- Brockett, C.L., Morgan, D.L.Proske, U., 2001. Human hamstring muscles adapt to eccentric exercise by changing optimum length. *Med Sci Sports Exerc* 33(5): 783-790.
- Brockett, C.L., Morgan, D.L.Proske, U., 2004. Predicting hamstring strain injury in elite athletes. *Medicine & Science in Sports & Exercise* 36(3): 379-387.
- Brooks, J.H., Fuller, C.W., Kemp, S.P.Reddin, D.B., 2006. Incidence, risk, and prevention of hamstring muscle injuries in professional rugby union. *Am J Sports Med* 34(8): 1297-1306.

- Butler, D.L., Juncosa, N., Dressler, M.R., 2004. Functional efficacy of tendon repair processes. *Annu Rev Biomed Eng* 6: 303-329.
- Butterfield, T.A., Herzog, W., 2005. Quantification of muscle fiber strain during in-vivo repetitive stretch-shortening cycles. *Journal of Applied Physiology* in press.
- Clark, R.A., 2008. Hamstring injuries: risk assessment and injury prevention. *Ann Acad Med Singapore* 37(4): 341-346.
- Connell, D.A., Schneider-Kolsky, M.E., Hoving, J.L., Malara, F., Buchbinder, R., Koulouris, G., Burke, F., Bass, C., 2004. Longitudinal study comparing sonographic and MRI assessments of acute and healing hamstring injuries. *AJR. American Journal of Roentgenology* 183(4): 975-984.
- Cooney, K.M., Sanders, J.O., Concha, M.C., Buczek, F.L., 2006. Novel biomechanics demonstrate gait dysfunction due to hamstring tightness. *Clinical Biomechanics* 21(1): 59-66.
- Croisier, J.L., 2004. Factors associated with recurrent hamstring injuries. *Sports Medicine* 34(10): 681-695.
- Croisier, J.L., Forthomme, B., Namurois, M.H., Vanderthommen, M., Crielaard, J.M., 2002. Hamstring muscle strain recurrence and strength performance disorders. *American Journal of Sports Medicine* 30(2): 199-203.
- Davy, D.T., Audu, M.L., 1987. A dynamic optimization technique for predicting muscle forces in the swing phase of gait. *J Biomech* 20(2): 187-201.
- De Smet, A.A., 1993. Magnetic resonance findings in skeletal muscle tears. *Skeletal Radiology* 22(7): 479-484.
- De Smet, A.A., Best, T.M., 2000. MR imaging of the distribution and location of acute hamstring injuries in athletes. *AJR Am J Roentgenol* 174(2): 393-399.
- Delp, S.L., Loan, J.P., Hoy, M.G., Zajac, F.E., Topp, E.L., Rosen, J.M., 1990. An interactive graphics-based model of the lower extremity to study orthopaedic surgical procedures. *IEEE Trans Biomed Eng* 37(8): 757-767.
- Delp, S.L., Loan, J.P., Hoy, M.G., Zajac, F.E., Topp, E.L., Rosen, J.M., 1990. An interactive graphics-based model of the lower extremity to study orthopaedic surgical procedures. *IEEE Transactions on Biomedical-Engineering* 37(8): 757-767.
- Drace, J.E., Pelc, N.J., 1994. Measurement of skeletal muscle motion in vivo with phase-contrast MR imaging. *Journal of Magnetic Resonance Imaging* 4: 157-163.
- Drace, J.E., Pelc, N.J., 1994. Skeletal muscle contraction: analysis with use of velocity distributions from phase-contrast MR imaging. *Radiology* 193(2): 423-429.
- Drape, J.L., Silbermann-Hoffman, O., Houvet, P., Dubert, T., Thivet, A., Benmelha, Z., Frot, B., Alnot, J.Y., Benacerraf, R., 1996. Complications of flexor tendon repair in the hand: MR imaging assessment. *Radiology* 198(1): 219-224.
- Edrich, T., Riener, R., Quintern, J., 2000. Analysis of passive elastic joint moments in paraplegics. *IEEE Transactions on Biomedical Engineering* 47(8): 1058-1065.
- Epstein, M., Herzog, W., 2003. Aspects of skeletal muscle modelling. *Philosophical Transactions of the Royal Society B: Biological Sciences* 358(1437): 1445-1452.

- Fernandez, J.W., Buist, M.L., Nickerson, D.P., Hunter, P.J., 2005. Modelling the passive and nerve activated response of the rectus femoris muscle to a flexion loading: a finite element framework. *Med Eng Phys* 27(10): 862-870.
- Finni, T., Hodgson, J.A., Lai, A.M., Edgerton, V.R., Sinha, S., 2003. Nonuniform strain of human soleus aponeurosis-tendon complex during submaximal voluntary contractions in vivo. *J Appl Physiol* 95(2): 829-837.
- Friden, J., Lieber, R.L., 1998. Segmental muscle fiber lesions after repetitive eccentric contractions. *Cell Tissue Res* 293(1): 165-171.
- Fukashiro, S., Hay, D.C., Nagano, A., 2006. Biomechanical behavior of muscle-tendon complex during dynamic human movements. *J Appl Biomech* 22(2): 131-147.
- Fukunaga, T., Kawakami, Y., Kubo, K., Kanehisa, H., 2002. Muscle and tendon interaction during human movements. *Exercise & Sport Sciences Reviews* 30(3): 106-110.
- Fukunaga, T., Kubo, K., Kawakami, Y., Fukashiro, S., Kanehisa, H., Maganaris, C.N., 2001. In vivo behaviour of human muscle tendon during walking. *Proc R Soc Lond B Biol Sci* 268(1464): 229-233.
- Garrett, W.E., Jr., 1990. Muscle strain injuries: clinical and basic aspects. *Medicine & Science in Sports & Exercise* 22(4): 436-443.
- Garrett, W.E., Jr., 1996. Muscle strain injuries. *American Journal of Sports Medicine* 24(6 Suppl): S2-8.
- Garrett, W.E., Jr., Rich, F.R., Nikolaou, P.K., Vogler, J.B., 3rd, 1989. Computed tomography of hamstring muscle strains. *Med Sci Sports Exerc* 21(5): 506-514.
- Garrett, W.E., Jr., Safran, M.R., Seaber, A.V., Glisson, R.R., Ribbeck, B.M., 1987. Biomechanical comparison of stimulated and nonstimulated skeletal muscle pulled to failure. *Am J Sports Med* 15(5): 448-454.
- Gibbs, N.J., Cross, T.M., Cameron, M., Houang, M.T., 2004. The accuracy of MRI in predicting recovery and recurrence of acute grade one hamstring muscle strains within the same season in Australian Rules football players. *Journal of Science & Medicine in Sport* 7(2): 248-258.
- Gold, G.E., Hargreaves, B.A., Vasanawala, S.S., Webb, J.D., Shimakawa, A.S., Brittain, J.H., Beaulieu, C.F., 2006. Articular Cartilage of the Knee: Evaluation with Fluctuating Equilibrium MR Imaging--Initial Experience in Healthy Volunteers. *Radiology* 238(2): 712-718.
- Heiderscheit, B.C., Hoerth, D.M., Chumanov, E.S., Swanson, S.C., Thelen, B.J., Thelen, D.G., 2005. Identifying the time of occurrence of a hamstring strain injury during treadmill running: a case study. *Clin Biomech (Bristol, Avon)* 20(10): 1072-1078.
- Hidler, J., Hodics, T., Xu, B., Dobkin, B., Cohen, L.G., 2006. MR compatible force sensing system for real-time monitoring of wrist moments during fMRI testing. *Journal of Neuroscience Methods* 155(2): 300-307.
- Holzbaur, K.R., Murray, W.M., Gold, G.E., Delp, S.L., 2007. Upper limb muscle volumes in adult subjects. *J Biomech* 40(4): 742-749.
- Hoy, M.G., Zajac, F.E., Gordon, M.E., 1990. A musculoskeletal model of the human lower extremity: the effect of muscle, tendon, and moment arm on the moment-angle

- relationship of musculotendon actuators at the hip, knee, and ankle. *J Biomech* 23(2): 157-169.
- Huijing, P.A., 2003. Muscular force transmission necessitates a multilevel integrative approach to the analysis of function of skeletal muscle. *Exerc Sport Sci Rev* 31(4): 167-175.
- Ishikawa, M., Komi, P.V., Grey, M.J., Lepola, V.Bruggemann, G.P., 2005. Muscle-tendon interaction and elastic energy usage in human walking. *Journal of Applied Physiology* 99(2): 603-608.
- Jarvinen, T.A., Jarvinen, T.L., Kaariainen, M., Kalimo, H.Jarvinen, M., 2005. Muscle injuries: biology and treatment. *Am J Sports Med* 33(5): 745-764.
- Jarvinen, T.A., Kaariainen, M., Jarvinen, M.Kalimo, H., 2000. Muscle strain injuries. *Current Opinion in Rheumatology* 12(2): 155-161.
- Jonhagen, S., Nemeth, G.Eriksson, E., 1994. Hamstring injuries in sprinters. The role of concentric and eccentric hamstring muscle strength and flexibility. *American Journal of Sports Medicine* 22(2): 262-266.
- Kaariainen, M., Jarvinen, T., Jarvinen, M., Rantanen, J.Kalimo, H., 2000. Relation between myofibers and connective tissue during muscle injury repair. *Scand J Med Sci Sports* 10(6): 332-337.
- Kaya, M., Jinha, A., Leonard, T.R.Herzog, W., 2005. Multi-functionality of the cat medical gastrocnemius during locomotion. *Journal of Biomechanics* 38(6): 1291-1301.
- Kerrigan, D.C., Todd, M.K., Della Croce, U., Lipsitz, L.A.Collins, J.J., 1998. Biomechanical gait alterations independent of speed in the healthy elderly: evidence for specific limiting impairments. *Arch Phys Med Rehabil* 79(3): 317-322.
- Kirkendall, D.T.Garrett, W.E., Jr., 2002. Clinical perspectives regarding eccentric muscle injury. *Clin Orthop* (403 Suppl): S81-89.
- Komi, P.V., 1984. Physiological and biomechanical correlates of muscle function: effects of muscle structure and stretch-shortening cycle on force and speed. *Exerc Sport Sci Rev* 12: 81-121.
- Koulouris, G.Connell, D., 2003. Evaluation of the hamstring muscle complex following acute injury. *Skeletal Radiology* 32(10): 582-589.
- Koulouris, G.Connell, D., 2005. Hamstring Muscle Complex: An Imaging Review 10.1148/rg.253045711. *Radiographics* 25(3): 571-586.
- Koulouris, G., Connell, D.A., Brukner, P.Schneider-Kolsky, M., 2007. Magnetic resonance imaging parameters for assessing risk of recurrent hamstring injuries in elite athletes. *Am J Sports Med* 35(9): 1500-1506.
- Krejci, V.Koch, P., 1979. Muscle and tendon injuries in athletes: diagnosis, treatment, muscle training, rehabilitation. *Year Book Medical Publishers, Chicago*.
- Kujala, U.M., Orava, S.Jarvinen, M., 1997. Hamstring injuries. Current trends in treatment and prevention. *Sports Medicine* 23(6): 397-404.
- Li, X.Aruin, A., 2005. Muscle activity onset time detection using teager-kaiser energy operator. *Conf Proc IEEE Eng Med Biol Soc* 7: 7549-7552.

- Lieber, R.L., Friden, J., 2002. Mechanisms of muscle injury gleaned from animal models. *Am J Phys Med Rehabil* 81(11 Suppl): S70-79.
- Lieber, R.L., Leonard, M.E., Brown, C.G., Trestik, C.L., 1991. Frog semitendinosus tendon load-strain and stress-strain properties during passive loading. *Am J Physiol* 261(1 Pt 1): C86-92.
- Lieber, R.L., Woodburn, T.M., Friden, J., 1991. Muscle damage induced by eccentric contractions of 25% strain. *J Appl Physiol* 70(6): 2498-2507.
- Lu, T.W., O'Connor, J.J., 1999. Bone position estimation from skin marker co-ordinates using global optimisation with joint constraints. *J Biomech* 32(2): 129-134.
- Mann, R.V., 1981. A kinetic analysis of sprinting. *Medicine & Science in Sports & Exercise* 13(5): 325-328.
- Mansour, J.M., Audu, M.L., 1986. The passive elastic moment at the knee and its influence on human gait. *Journal of Biomechanics* 19(5): 369-373.
- May, D.A., Disler, D.G., Jones, E.A., Balkissoon, A.A., Manaster, B.J., 2000. Abnormal signal intensity in skeletal muscle at MR imaging: patterns, pearls, and pitfalls. *Radiographics* 20 Spec No: S295-315.
- McGibbon, C.A., 2003. Toward a better understanding of gait changes with age and disablement: neuromuscular adaptation. *Exercise & Sport Sciences Reviews* 31(2): 102-108.
- Muraoka, T., Chino, K., Muramatsu, T., Fukunaga, T., Kanehisa, H., 2005. In vivo passive mechanical properties of the human gastrocnemius muscle belly. *Journal of Biomechanics* 38(6): 1213-1219.
- Nikolaou, P.K., Macdonald, B.L., Glisson, R.R., Seaber, A.V., Garrett, W.E., Jr., 1987. Biomechanical and histological evaluation of muscle after controlled strain injury. *Am J Sports Med* 15(1): 9-14.
- Noonan, T.J., Garrett, W.E., Jr., 1999. Muscle strain injury: diagnosis and treatment. *J Am Acad Orthop Surg* 7(4): 262-269.
- Novacheck, T.F., 1998. The biomechanics of running. *Gait & Posture* 7: 77-95.
- Orchard, J., Best, T.M., 2002. The management of muscle strain injuries: an early return versus the risk of recurrence. *Clinical Journal of Sport Medicine* 12(1): 3-5.
- Orchard, J., Marsden, J., Lord, S., Garlick, D., 1997. Preseason hamstring muscle weakness associated with hamstring muscle injury in Australian footballers. *Am J Sports Med* 25(1): 81-85.
- Orchard, J., Seward, H., 2002. Epidemiology of injuries in the Australian Football League, seasons 1997-2000. *Br J Sports Med* 36(1): 39-44.
- Orchard, J.W., 2001. Intrinsic and extrinsic risk factors for muscle strains in Australian football. *American Journal of Sports Medicine* 29(3): 300-303.
- Ounpuu, S., 1990. The biomechanics of running: a kinematic and kinetic analysis. *Instr Course Lect* 39: 305-318.
- Pappas, G.P., Asakawa, D.S., Delp, S.L., Zajac, F.E., Drace, J.E., 2002. Nonuniform shortening in the biceps brachii during elbow flexion. *J Appl Physiol* 92(6): 2381-2389.

- Paton, R.W., Grimshaw, P., McGregor, J.Noble, J., 1989. Biomechanical assessment of the effects of significant hamstring injury: an isokinetic study. *J Biomed Eng* 11(3): 229-230.
- Pelc, N.J., Drangova, M., Pelc, L.R., Zhu, Y., Noll, D.C., Bowman, B.S.Herfkens, R.J., 1995. Tracking of cyclic motion with phase-contrast cine MR velocity data. *J Magn Reson Imaging* 5(3): 339-345.
- Piazza, S.J., Erdemir, A., Okita, N.Cavanagh, P.R., 2004. Assessment of the functional method of hip joint center location subject to reduced range of hip motion. *J Biomech* 37(3): 349-356.
- Pinniger, G.J., Steele, J.R.Groeller, H., 2000. Does fatigue induced by repeated dynamic efforts affect hamstring muscle function? *Med Sci Sports Exerc* 32(3): 647-653.
- Proske, U., Morgan, D.L., Brockett, C.L.Percival, P., 2004. Identifying athletes at risk of hamstring strains and how to protect them. *Clinical & Experimental Pharmacology & Physiology* 31(8): 546-550.
- Purslow, P.P., 2002. The structure and functional significance of variations in the connective tissue within muscle. *Comp Biochem Physiol A Mol Integr Physiol* 133(4): 947-966.
- Reeder, S.B., Pineda, A.R., Wen, Z., Shimakawa, A., Yu, H., Brittain, J.H., Gold, G.E., Beaulieu, C.H.Pelc, N.J., 2005. Iterative decomposition of water and fat with echo asymmetry and least-squares estimation (IDEAL): application with fast spin-echo imaging. *Magn Reson Med* 54(3): 636-644.
- Reeves, N.D.Narici, M.V., 2003. Behavior of human muscle fascicles during shortening and lengthening contractions in vivo. *J Appl Physiol* 95(3): 1090-1096.
- Riener, R.Edrich, T., 1999. Identification of passive elastic joint moments in the lower extremities. *Journal of Biomechanics* 32(5): 539-544.
- Rybak, L.D.Torriani, M., 2003. Magnetic resonance imaging of sports-related muscle injuries. *Top Magn Reson Imaging* 14(2): 209-219.
- Schneider-Kolsky, M.E., Hoving, J.L., Warren, P.Connell, D.A., 2006. A comparison between clinical assessment and magnetic resonance imaging of acute hamstring injuries. *Am J Sports Med* 34(6): 1008-1015.
- Seward, H., Orchard, J., Hazard, H.Collinson, D., 1993. Football injuries in Australia at the elite level. *Med J Aust* 159: 298-301.
- Sheehan, F.T., Zajac, F.E.Drace, J.E., 1998. Using cine phase contrast magnetic resonance imaging to non-invasively study in vivo knee dynamics. *J Biomech* 31(1): 21-26.
- Shellock, F.G., 2002. Magnetic resonance safety update 2002: implants and devices. *J Magn Reson Imaging* 16(5): 485-496.
- Sherry, M.Best, T., 2004. A comparison of two rehabilitation programs in the treatment of acute hamstring strains. *Journal of Orthopaedic & Sports Physical Therapy* 34(3): 116-125.
- Silder, A., Heiderscheit, B.C., Thelen, D.G., Enright, T.Tuite, M.J., 2008. MR observations of long-term musculotendon remodeling following a hamstring strain injury. *Skeletal Radiol* DOI: 10.1007/s00256-008-0546-0.

- Silder, A., Heiderscheit, B.C., Thelen, D.G., Enright, T., Tuite, M.J., 2008. MR observations of long-term musculotendon remodeling following a hamstring strain injury. *Skeletal Radiol* 37(12): 1101-1109.
- Silder, A., Thelen, D.G., 2009. The Influence of Prior Hamstring Injury on Musculotendon Morphology and Muscle Contraction Mechanics American Society of Biomechanics Annual Meeting, Penn State University,
- Silder, A., Westphal, C., Thelen, D., 2009. Device Paper.
- Silder, A., Westphal, C., Thelen, D., 2009. A MR-Compatible Loading Device for Dynamically Imaging Shortening and Lengthening Muscle Contraction Mechanics. *J Med Devices* In Press.
- Silder, A., Whittington, B., Heiderscheit, B., Thelen, D.G., 2007. Identification of passive elastic joint moment-angle relationships in the lower extremity. *J Biomech* 40(12): 2628-2635.
- Slavotinek, J.P., Verrall, G.M., Fon, G.T., 2002. Hamstring injury in athletes: using MR imaging measurements to compare extent of muscle injury with amount of time lost from competition. *AJR. American Journal of Roentgenology* 179(6): 1621-1628.
- Speer, K.P., Lohnes, J., Garrett, W.E., Jr., 1993. Radiographic imaging of muscle strain injury. *Am J Sports Med* 21(1): 89-95; discussion 96.
- Thelen, D.G., Chumanov, E.S., Best, T.M., Swanson, S.C., Heiderscheit, B.C., 2005. Simulation of biceps femoris musculotendon mechanics during the swing phase of sprinting. *Med Sci Sports Exerc* 37(11): 1931-1938.
- Thelen, D.G., Chumanov, E.S., Hoerth, D.M., Best, T.M., Swanson, S.C., Li, L., Young, M., Heiderscheit, B.C., 2005. Hamstring muscle kinematics during treadmill sprinting. *Med Sci Sports Exerc* 37(1): 108-114.
- Thelen, D.G., Chumanov, E.S., Sherry, M.A., Heiderscheit, B.C., 2006. Neuromusculoskeletal models provide insights into the mechanisms and rehabilitation of hamstring strains. *Exerc Sport Sci Rev* 34(3): 135-141.
- Tingart, M.J., Apreleva, M., Lehtinen, J.T., Capell, B., Palmer, W.E., Warner, J.J., 2003. Magnetic resonance imaging in quantitative analysis of rotator cuff muscle volume. *Clin Orthop Relat Res* (415): 104-110.
- Tuite, M.J., DeSmet, A.A., 1994. MRI of selected sports injuries: muscle tears, groin pain, and osteochondritis dissecans. *Seminars in Ultrasound, CT & MR* 15(5): 318-340.
- Verrall, G.M., Slavotinek, J.P., Barnes, P.G., Fon, G.T., Esterman, A., 2006. Assessment of physical examination and magnetic resonance imaging findings of hamstring injury as predictors for recurrent injury. *J Orthop Sports Phys Ther* 36(4): 215-224.
- Verrall, G.M., Slavotinek, J.P., Barnes, P.G., Fon, G.T., Spriggins, A.J., 2001. Clinical risk factors for hamstring muscle strain injury: a prospective study with correlation of injury by magnetic resonance imaging. *British Journal of Sports Medicine* 35(6): 435-439; discussion 440.
- Vrahas, M.S., Brand, R.A., Brown, T.D., Andrews, J.G., 1990. Contribution of passive tissues to the intersegmental moments at the hip. *Journal of Biomechanics* 23(4): 357-362.

- Walker, P.S., Rovick, J.S., Robertson, D.D., 1988. The effects of knee brace hinge design and placement on joint mechanics. *J Biomech* 21(11): 965-974.
- Warren, P., Gabbe, B.J., Schneider-Kolsky, M., Bennell, K.L., 2008. Clinical predictors of time to return to competition and of recurrence following hamstring strain in elite Australian footballers. *Br J Sports Med*.
- Whittington, B.R., Thelen, D.G., 2009. A simple mass-spring model with roller feet can induce the ground reactions observed in human walking. *J Biomech Eng* 131(1): 011013.
- Wood, G., 1987. Biomechanical limitations to sprint running. *Med Sci Sports Exerc* 25: 58-71.
- Woodley, S.J., Mercer, S.R., Hamstring strains - Where do they occur?
- Woods, C., Hawkins, R.D., Maltby, S., Hulse, M., Thomas, A., Hodson, A., 2004. The Football Association Medical Research Programme: an audit of injuries in professional football--analysis of hamstring injuries. *Br J Sports Med* 38(1): 36-41.
- Worrell, T., Perrin, D., Gansneder, B., Gieck, J., 1991. Comparison of isokinetic strength and flexibility measures between hamstring injured and noninjured athletes. *J Ortho Sport Phys Therapy* 13(3): 118-125.
- Yoon, Y.S., Mansour, J.M., 1982. The passive elastic moment at the hip. *Journal of Biomechanics* 15(12): 905-910.
- Yucesoy, C.A., Huijing, P.A., 2007. Substantial effects of epimuscular myofascial force transmission on muscular mechanics have major implications on spastic muscle and remedial surgery. *J Electromyogr Kinesiol* 17(6): 664-679.
- Zajac, F.E., 1989. Muscle and tendon: properties, models, scaling, and application to biomechanics and motor control. *Critical Reviews in Biomedical Engineering* 17(4): 359-411.
- Zhong, X., Epstein, F.H., Spottiswoode, B.S., Helm, P.A., Blemker, S.S., 2008. Imaging two-dimensional displacements and strains in skeletal muscle during joint motion by cine DENSE MR. *J Biomech* 41(3): 532-540.
- Zhou, H., Novotny, J.E., 2007. Cine phase contrast MRI to measure continuum Lagrangian finite strain fields in contracting skeletal muscle. *J Magn Reson Imaging* 25(1): 175-184.
- Zhu, Y., Drangova, M., Pelc, N.J., 1996. Fourier tracking of myocardial motion using cine-PC data. *Magn Reson Med* 35(4): 471-480.
- Zhu, Y., Pelc, N.J., 1999. A spatiotemporal model of cyclic kinematics and its application to analyzing nonrigid motion with MR velocity images. *IEEE Trans Med Imaging* 18(7): 557-569.

APPENDIX A

A mathematical model was used to describe the relationship between the sagittal plane joint angles and passive joint moments about the hip (h), knee (k), and ankle (a). The model included five uni-articular and three bi-articular components. The uni-articular components account for the net moments generated via the single-joint dependent stretch of soft tissue such as ligaments, skin, relaxed uni-articular musculotendons, and the joint capsule. The uni-articular components in the model were divided into the hip flexors (HF), hip extensors (HE), knee flexors (KF), knee extensors (KE), and ankle plantarflexors (PF). The passive ankle dorsiflexor moments were not included since they are not thought to contribute substantially during human gait. The bi-articular muscles in the model were the rectus femoris (RF), hamstrings (HAM), and gastrocnemius (GAS). Model inputs included experimentally measured hip, knee, and ankle angles (θ_{joint}) and joint moments.

Each uni-articular component was represented by an exponential function parameterized by a gain (β) and offset angle (α)

$$\hat{M} = e^{\beta(\theta - \alpha)} \quad (\text{A.1})$$

where θ is the measured angle of the joint of interest. Note that the predicted uni-articular moment, \hat{M} , reduces to a value of 1 Nm when the joint angle θ is equal to the offset angle α .

Bi-articular muscles generate moments about both the proximal and distal joints they span, and thus have the potential to do simultaneous positive or negative work at

either joint while also storing or releasing energy. We formulated the passive bi-articular functions to allow such energy transfer between joints, while ensuring that net energy was neither lost nor created. In general, energy conservation is ensured when the joint moments are the differential of a potential energy function with respect to the proximal (*prox*) or distal (*dist*) joint angle. Defining the potential energy function as

$$E = \frac{1}{\beta_{prox}} e^{\beta_{prox}(\theta_{prox} - (\beta_{dist}/\beta_{prox})\theta_{dist} - \alpha_{prox})} \quad (A.2)$$

and differentiating with respect to the proximal and distal angles results in the following expressions used to represent the bi-articular joint moment-angle relationships.

$$\hat{M}_{prox} = e^{\beta_{prox}(\theta_{prox} - (\beta_{dist}/\beta_{prox})\theta_{dist} - \alpha_{prox})} \quad (A.3)$$

$$\hat{M}_{dist} = \left(\frac{\beta_{dist}}{\beta_{prox}} \right) e^{\beta_{prox}(\theta_{prox} - (\beta_{dist}/\beta_{prox})\theta_{dist} - \alpha_{prox})} \quad (A.4)$$

Bi-articular offset angles were described with respect to the muscle's more proximal joint (i.e. the value of α^{RF} could be directly compared to θ_h). The ratio, $\beta_{dist}/\beta_{prox}$, can be interpreted as the instantaneous ratio of the distal and proximal moment arms of a bi-articular muscle. For the bi-articular case, the passive moment reduces to a value of 1 Nm when the distal joint angle is zero and proximal joint angle is at the offset angle.

Considering the joints that each of the uni- and bi-articular components crosses, one obtains the following model for predicting the hip (\hat{M}_h), knee (\hat{M}_k), and ankle (\hat{M}_a) moments from the experimentally measured hip, knee, and ankle angles. A total of

19 parameters were used in the model including 11 gain constants (β_{joint}^{muscle}) and 8 offset angles (α^{muscle}).

$$\begin{aligned} \hat{M}_h = & e^{-\beta_h^{RF}(\theta_h - (\beta_k^{RF}/\beta_h^{RF})\theta_k - \alpha^{RF})} + e^{-\beta_h^{HF}(\theta_h - \alpha^{HF})} \\ & - e^{\beta_h^{HAM}(\theta_h - (\beta_k^{HAM}/\beta_h^{HAM})\theta_k - \alpha^{HAM})} - e^{\beta_h^{HE}(\theta_h - \alpha^{HE})} \end{aligned} \quad (A.5)$$

$$\begin{aligned} \hat{M}_k = & -\left(\frac{\beta_k^{RF}}{\beta_h^{RF}}\right) e^{-\beta_h^{RF}(\theta_h - (\beta_k^{RF}/\beta_h^{RF})\theta_k - \alpha^{RF})} - e^{\beta_k^{KE}(\theta_k - \alpha^{KE})} \\ & + \left(\frac{\beta_k^{HAM}}{\beta_h^{HAM}}\right) e^{\beta_h^{HAM}(\theta_h - (\beta_k^{HAM}/\beta_h^{HAM})\theta_k - \alpha^{HAM})} \\ & + e^{-\beta_k^{KF}(\theta_k - \alpha^{KF})} + e^{\beta_k^{GAS}(\theta_k - (\beta_a^{GAS}/\beta_k^{GAS})\theta_a - \alpha^{GAS})} \end{aligned} \quad (A.6)$$

$$\hat{M}_a = -\left(\frac{\beta_a^{GAS}}{\beta_k^{GAS}}\right) e^{\beta_k^{GAS}(\theta_k - (\beta_a^{GAS}/\beta_k^{GAS})\theta_a - \alpha^{GAS})} - e^{\beta_a^{PF}(\theta_a - \alpha^{PF})} \quad (A.7)$$

Model parameters were estimated by determining the set of parameters that minimized the sum of squared errors between model-predicted and measured moments over all passive motion trials.

APPENDIX B

<u>Breakfast</u>	<u>Brand</u>
Hot Chocolate	Swiss Miss
Fat Free Cool Whip	Cool Whip
Vanilla Whipped Frosting	Pillsbury
Vanilla Ice Cream	Walgreens
Lite Yogurt	Yoplait

Pre-workout meal: Spread a thin layer of frosting onto your choice of cookie, ½ Pop Tart, or partial rice crispy treat and enjoy.

Post-workout meal: Combine two rounded spoons of hot chocolate with 8oz. of milk and 6oz of yogurt into a Nalgene water bottle. Fill the rest of the water bottle with boiling water. Shake thoroughly.

<u>Snack #1</u>	<u>Brand</u>
Cookie Crisp Cereal	Kellogg's
Peanut Butter Puffs Cereal	Kellogg's or General Mills
Sea Foam Candy	N/A

Suggestions: Combine cereal into a bowl, break up sea foam candy, and enjoy. Add additional chocolate based candy, broken up cookies, and/or Pop Tarts if desired.

<u>Lunch</u>	<u>Brand</u>
Cracklin' Oat Bran	Kellogg's
Circus Peanuts	N/A
Malted Milk Balls	Whoppers

Suggestions: Combine cereal and Malted Milk Balls into a bowl. Add chocolate based candy, broken up cookies, Pop Tarts, and/or malted milk balls if desired. Eat Circus Peanuts separately with a clean empty mouth.

<u>Snack #2</u>	<u>Brand</u>
Blueberry Muffin Tops Cereal	Woodman's
Jelly Beans	Generic

<u>Supper</u>	<u>Brand</u>
Vidalia Onion	N/A
Mushrooms	N/A
Cabbage or Lettuce	N/A
Fat Free Cottage Cheese	Deans
Fake Crab Mean – flake style	N/A
Baby Carrots	N/A
Red Tomatoes	N/A
Corn on the Cob	N/A
Hot Dogs	Ball Park
Kosher Spear Pickles	Vlasic
Cheese and Alfredo Spaghetti Sauce	Ragu
Macaroni and Cheese	Kraft

Suggestions: Shred cabbage. Combine cabbage or lettuce, chopped mushrooms, chopped Vidalia onion, baby carrots, and chopped red tomatoes into a bowl. Add cottage cheese and your choice of chopped hot dogs or fake crab meat into the bowl. Pour cheese or alfredo spaghetti sauce into the mix and stir.

<u>Desert</u>	<u>Brand</u>
Cookies and Crème Ice Cream	Walgreens
Take the Cake Ice Cream	Edy's
French Toast Sticks	Market Day